CONTRIBUTIONS TO THE SCIENCE MODELING REQUIREMENTS DOCUMENT

EARTH LIMB & AURORAL BACKGROUNDS

C. I. Meng
Johns Hopkins University
Applied Physics Laboratory

R. R. O'Neil
Geophysics Laboratory
Hanscom Air Force Base

October 1990

Accession Number: 6334

Publication Date: Oct 01, 1990

Title: Contributions To The MSX Science Requirements Document: Earth Limb And Auroral Backgrounds

Personal Author: Meng, C.I.; O'Neil, R.R.

Corporate Author Or Publisher: Johns Hopkins University, Applied Physics Laboratory, Laurel, MD; Geophysics Laboratory, Hanscom AFB, MA

Comments on Document: from BMDO/DE

Abstract: SDI systems must acquire and track targets such as rockets, PBVs, and RVs as they traverse the atmosphere between ground level and altitudes of about 1800 km. To distinguish between target and background, these system require an accurate model of terrestrial background scenes. The models in turn require knowledge of atmospheric species, temperatures, dynamics, and structures. In addition, the targets' interactions with th atmosphere will provide detection and discrimination methods that can be evaluated only by using models incorporating realistic atmospheric models. To satisfy these needs, MSX will thoroughly measure the earth's background radiation. These measurements encompass those of the earth limb, the aurora, and the hard earth. The background measurements will span the entire lifetime of the MSX mission.

Descriptors, Keywords: earth limb aurora background MSX experiment model requirement infrared short limb terrestrial background atmospherics neutral atmosphere ionosphere emission radiance transmittance dynamics clutter airglow mesospheric cloud segmentation

Pages: 68

Cataloged Date: Jan 07, 1998

Copyrighted or Not: NO

Document Type: HC

Number of Copies In Library: 000001

Record ID: 46052

Source of Document: BMD

Contributions to the MSX Science
Modeling Requirements Document

EARTH LIMB & AURORAL BACKGROUNDS

C. I. Meng
Johns Hopkins University
Applied Physics Laboratory

R. R. O'Neil
Geophysics Laboratory
Hanscom Air Force Base

October 1990

This document was compiled and merged by members of the Short Wavelength Terrestrial Background Team and the Infrared Earth Limb and Aurora Team for the MSX Science Modeling Requirements Document

CONTENTS

LIST OF FIGURES AND TABLES FOR SECTION 4

4. EARTH LIMB & AURORAL BACKGROUNDS

4.1. INTRODUCTION

SDI systems must acquire and track targets such as rockets, PBVs and RVs as they traverse the atmosphere between ground level and altitudes of ~1800 km. To distinguish between target and background, these systems require an accurate models of terrestrial background scenes. The models in turn require knowledge of atmospheric species, temperatures, dynamics, and structures. In addition, the targets' interactions with the atmosphere will provide detection and discrimination methods that can be evaluated only by using models incorporating realistic atmospheric models. To satisfy these needs, MSX will thoroughly measure the Earth's background radiation. These measurements encompass those of the Earth limb, the aurora, and the hard Earth. The background measurements will span the entire lifetime of the MSX mission.

This section discusses the science requirements for the Earth backgrounds measurements comprehended by MSX. The section begins by discussing the state of the available databases and models, emphasizing the deficiencies in the state of the art. The section then outlines those measurements required for MSX in order to supplement the present state of knowledge of Earth backgrounds. The section concludes by discussing the impact MSX measurements will have.

MSX's wide coverage in wavelength ensures the observation of a multitude of atmospheric emissions (Table 4-1). Together, the observation of these radiations allows the investigation of a multitude of strategically relevant background phenomena such as auroral surges, polar mesospheric clouds, and atmospheric structure. A basic synergy exists between the infrared, the visible and the ultraviolet. Each wavelength domain offers a unique perspective on the Earth's background, and each contributes to the interpretation of the other's observations.

Table 4-1
RELEVANT ATMOSPHERIC EMISSIONS

Emission	λ (μm)	comment
H Lyman α	0.1216	geocorona
O	0.1304	airglow/aurora
O	0.1356	airglow/aurora
N_2 VK	0.220-0.340	aurora
N_2 LBH	0.130-0.200	aurora
NO γ	0.200-0.250	airglow
O_2 Herzberg I	0.270-0.300	nightglow at ~90 km
N_2^+ 1N	0.3914 et al.	airglow/aurora
O (^{1}S)	0.5577	airglow/aurora
Na	0.5890	bright airglow layer at 92 km
O (^{3}D)	0.6300	airglow
O_2 Atm	0.650-0.900	aurora
O_2 Atm IR	1.25-1.60	aurora
NO	2.7	first overtone, above 70 km
H_2O (v_1, v_3)	2.7	
OH	2.7	airglow, spacecraft glow
CO_2 (v_3)	4.3	airglow
N_2O	4.5	
CO	4.6	
O_3	4.8	ozone monitor
NO	5.3	
N_2O	6.2	
H_2O (v_2)	6.3	
N_2O	7.8	
O_3 (v_3)	9.6	ozone monitor
CO_2 (v_2)	15	airglow
H_2O	16-25	rotational bands
N_2O	17	

4.2. STATE OF MODERN RESEARCH

4.2.1. NEUTRAL ATMOSPHERE

Regardless of wavelength regime, all models of atmospheric background radiation *must* utilize accurate information about the neutral atmosphere. Indeed, the state of the terrestrial atmosphere essentially *defines* the terrestrial background radiation and determines strategically relevant parameters such as background clutter, time scales, and radiance levels.

Models of the neutral atmosphere provide temperature, pressure, and composition information. All models give these parameters as functions of altitude. Depending on its sophistication, a model may also report these parameters as averages or as functions of latitude and longitude, local time and universal time (UT), and solar and geomagnetic activity. This discussion concentrates on the middle and upper atmosphere (h>60 km), which includes the mesosphere and thermosphere, because most MSX observations pertain to these altitude regimes. Figure 4-1 exhibits an example of profiles derived from typical models of the atmosphere.

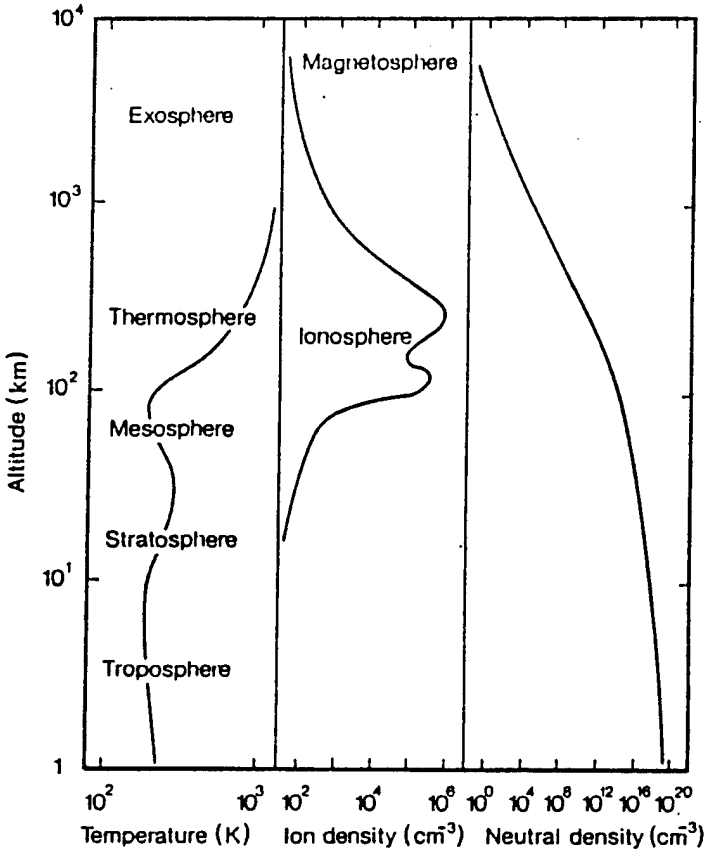

Fig. 4-1. Schematic representation of the thermal structure, the ion density, and the neutral density of the Earth's atmosphere. The approximate altitude regimes of various atmospheric regions are indicated. (from Rees, 1989).

Four principal models of the neutral atmosphere have emerged: the United States Standard Atmosphere (USSA), the COSPAR International Reference Atmosphere (CIRA), the Jacchia model atmosphere, and the Mass Spectrometer and Incoherent Scatter (MSIS) model atmosphere. The USSA and CIRA models were developed by large standing committees of experts and have undergone extensive revision over several decades. The Jacchia and MSIS models essentially represent efforts of principal investigators leading comparatively small teams of researchers.

The USSA is a total density model of the atmosphere. The model has undergone several major revisions since it first appeared in the early 1960's (COESA, 1962, 1965, 1976). In its most recent incarnation, USSA provides temperature in the form of approximate analytic functions, valid up to 200 km, from which pressure and density are computed. The model divides the atmosphere into a lower part below 120 km and an upper part above 120 km and is supposedly valid to 1000 km. The lower part includes seasonal and latitudinal variations, while the upper part incorporates the effects of solar activity, geomagnetic activity (through the A_p index), and solar zenith angle. USSA also contains compositional profiles of major species (O_2, O, N_2) and minor species (O_3, Ar, NO, NO_2, H_2S, SO_2, CO, CO_2, NH_3, CH_4) as well as aerosols (particulates). The latest version extends over a complete solar cycle (22 years). The various revisions of USSA have applied only to the atmosphere above ~50 km; the model of the lower atmosphere has remained essentially intact since 1962.

The COSPAR International Reference Atmosphere (CIRA) has a similar history and vintage as USSA. The initial version of CIRA (COSPAR, 1961) incorporated total density data and computational mechanisms similar to that of USSA-1962. Later versions of CIRA, however, simply adopted published versions of other models. CIRA-1965 (COSPAR, 1965) appropriated the model developed by Harris and Priester (1962a,b) which solved a heat conduction equation to determine exospheric temperatures. CIRA-1972 (COSPAR, 1972) adopted the total density model of Jacchia (1972), which relied on satellite drag data. The latest version, CIRA-1986 (COSPAR, 1986) is merely the MSIS compositional model of Hedin (1983).

L.G. Jacchia of the Smithsonian Astrophysical Observatory developed a third series of atmospheric models (often designated by "J" + year) based on satellite drag data. The initial Jacchia model determined density and scale height as functions of altitude and solar activity (as reflected in F_{20} fluxes) (Jacchia, 1960). J65 model included the five principal types of thermospheric density variations (diurnal, seasonal, semi-annual, solar activity, and magnetic activity) and computed height profiles of principle components assuming diffusive equilibria above 120 km (Jacchia, 1965). The J70 model extended J65 down to 90 km, employed more sophisticated temperature profiles, and added a winter bulge in He density (Jacchia, 1970). The J71 model contrived O densities to agree with rocket measurements and used height-dependent density variations rather than semi-annual temperature variations (Jacchia, 1971). The final J77 model extensively revised J71 by

improving the approximation to diurnal variations and magnetic activity and including seasonal-latitudinal variations of N_2 and O (Jacchia, 1977; Jacchia et al., 1978).

The MSIS models derive from the compositional data of mass spectrometers and incoherent scatter radars and have largely been the work of A.E. Hedin of Goddard Spaceflight Center. The MSIS model originated with a global-empirical model derived from the OGO-6 mass spectrometer (Hedin et al., 1973, 1974). This initial model fit longitudinal averages of N_2, O, and He to a spherical harmonic expansion and included diurnal, semi-diurnal, terdiurnal, annual, and semiannual terms. The model also allowed for solar flux (using the $F_{10.7}$ index) and geomagnetic activity (using the A_p index). The MSIS-77 model (Hedin et al., 1977a,b) expanded its database to five satellites and four ground-based incoherent scatter radars. A revised MSIS-77 took into account longitudinal and UT variations in thermospheric composition and temperature (Hedin et al., 1979). MSIS-83 expanded the database to include rocket mass spectrometer and UV absorption measurements of atmospheric parameters (Hedin, 1983). MSIS-83 modeled magnetic storm variations in terms of the 3hr ap index and extended its region of validity down to the mesopause (~85 km). MSIS-86 brought the model essentially to its present form by including new data from the DE satellite, which improved coverage in the polar regions for both disturbed and quiet times (Hedin, 1987). MSIS-86 also included atomic nitrogen in its composition profiles.

The various atmospheric models have undergone considerable validation, both in relation to measurements and to each other. For example, the J77 and MSIS-86 models generally agreed to within ~15% ion predicting O densities (Hedin, 1988). Differences result primarily from variations caused by magnetic storms, EUV radiation, geographical effects, and small scale variations such as gravity waves. Hedin and Thuiller (1988) compared OGO-6 measurements of thermospheric temperature (derived from optical data) with those predicted by MSIS-86 (derived from mass spectrometer and radar data) and found good agreement except near the South Atlantic anomaly and near local noon (the latter discrepancy caused by an instrument problem). Specifically, MSIS-86 predicted the yearly average temperature to within 16K, the solstice temperatures, and the high-latitude magnetic activity variations.

Each of these neutral atmosphere models has or had a specific part to play in the study of terrestrial background radiation. The USSA and CIRA have become the standard model for study of the lower atmosphere below ~85 km, while the many IR limb models have adopted the CIRA model atmosphere for use above ~60 km. The MSIS-86 model has become the standard for use in the thermospheric research above ~85 km. Hedin (1988) suggests that the J77 model may still be valid for estimating satellite drag effects, but that investigators should utilize the MSIS model for aeronomical calculations.

These models have served the research community admirably yet suffer from several deficiencies. First, the models have limited ranges of

validity. For example, general models of the atmosphere such as USSA or MSIS accurately describe conditions only within certain altitudinal and latitudinal regimes. A paucity of observations exists especially at high latitudes and at altitudes near the mesopause (~80-90 km), places where long-term in-situ measurements are difficult to make. Second, essentially all of atmospheric models rely on data that represent statistical averages of single-point measurements. Such measurements present a spatially or temporally biased view of the phenomenon under consideration. Interpolation between points of measurement may not produce the correct information, especially at high latitudes or in the auroral region. Third, the empirical models may derive from limited or obsolete databases. In large part, the USSA uses data obtained during the 1950's, while MSIS uses data taken during part of one solar cycle.

4.2.2. IONOSPHERE

The complete description of terrestrial atmospheric radiation also requires understanding of the charged particle environment, or ionosphere. For example, interactions between ions and electrons generate metastable species that radiate at virtually all wavelengths from the ultraviolet through the longwave infrared. Furthermore, Joule heating that results from neutral-ion collisions can increase temperatures and affect the infrared background scene. Finally, motions of the ionosphere induce motions of the neutral atmosphere (especially at high altitudes) and generate complex patterns of the background clutter.

Models of the terrestrial ionosphere attempt primarily to predict the altitudinal profiles of electron density (n_e) or total electron content (TEC), the maximum electron density (n_{max}), the altitude of the peak electron density (h_{max}), the ion density or composition (n_i), and the electron and ion temperatures (T_e and T_i). The models must take into account a wide range of effects such as solar EUV radiation, geomagnetic activity, solar activity, diurnal changes, dynamical motions, and coupling between the neutral and ionized components (see Fig. 4-2). Ionospheric models must accommodate magneto-hydrodynamics rather than merely hydrodynamics, as do neutral atmosphere models. In practice, the models of the ionosphere rely on the fitting empirical data to expansion functions and so resemble models of the neutral atmosphere.

Two commonly used models of the ionosphere are the International Reference Ionosphere (IRI) and the Ionospheric Conductivity and Electron Density (ICED) model. The IRI group within COSPAR has developed an ionospheric model to complement the CIRA model of the neutral atmosphere. The group supervises the gathering and reviewing of basic ionospheric data and establishes approved profiles of ionospheric parameters such as n_e, T_e, n_i, and T_i (e.g., Rawer et al., 1981,1984). These parameters are binned by geomagnetic activity, local time, latitude and longitude, etc. The model itself represents a massive database of measurements made by a variety of instruments at different locations and under different levels of geomagnetic

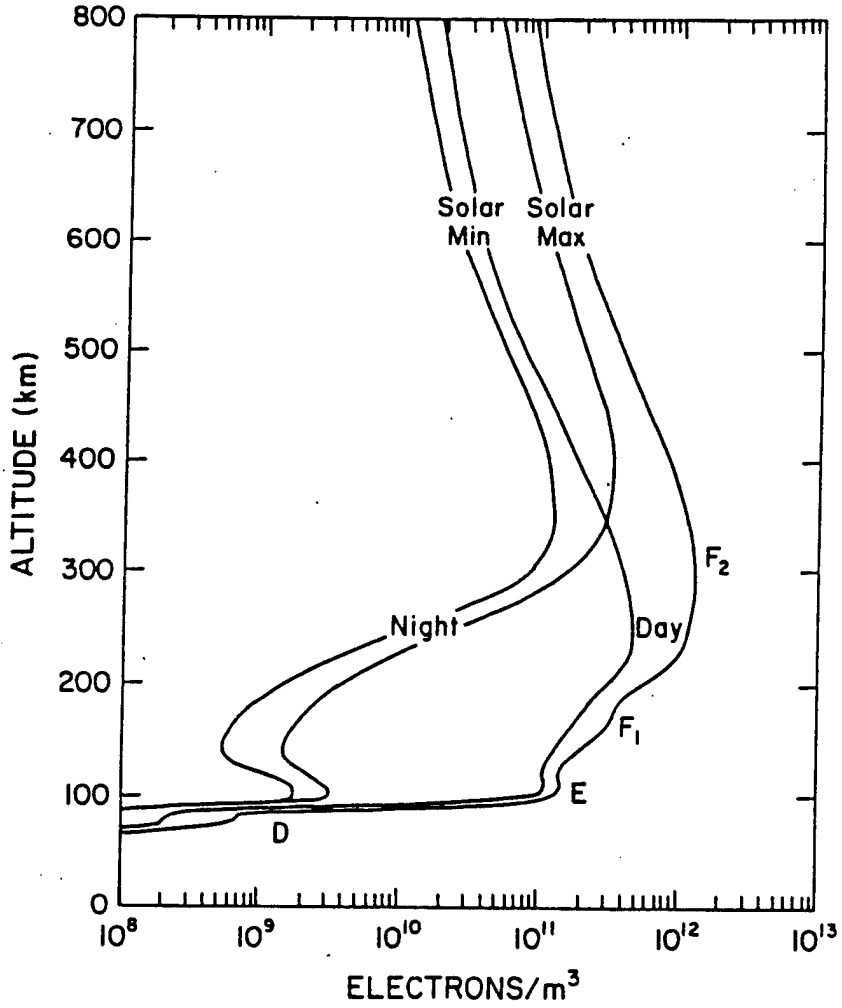

Fig. 4-2. Typical midlatitude electron density profiles for sunspot maximum and minimum, day and night. Different regions of the ionosphere are labelled D,E,F_1 and F_2.

and solar activity. The potential user usually accesses IRI from a computer program. COSPAR intends that IRI serve as a standard reference for the ionosphere, just as CIRA would for the neutral atmosphere (e.g., Rawer et al., 1978). Like the models of the neutral atmosphere, the IRI model has undergone several revisions and continues to develop as new measurements become available.

The Ionospheric Conductivity and Electron Density (ICED) model (Kroehl and Hausman, 1986) generates the global distribution of electron densities as a function of time, altitude, geographic latitude and longitude, and geomagnetic and solar activity. The user specifies a grid, sunspot number and geomagnetic index (Q), and the ICED program responds by computing the corresponding ionospheric morphology (polar cap boundary, auroral zone, etc.) and electron profile at each grid point. These computations proceed by fitting data to parabolic and Chapman functions. This scheme allows flexibility in the choice of fitting functions and databases but does not solve

Maxwell's equations nor include plasma transport effects (except where they are statistically definable). The resulting electron profiles extend from 90km to 500km in 10km increments and from 500km to 1000km in 50km increments. Current versions of the model (ICED-86-II) do not include the dynamics of plasma transport, but do flag regions where this might occur and invalidate the model. ICED serves as an operational forecasting program of USAF Global Weather Central.

Ionospheric models suffer from deficiencies similar to those that affect neutral atmosphere models. They are statistical models only and cannot describe instantaneous conditions no matter how accurately an input parameter is specified. Thus, IRI and ICED may not accurately model regions that undergo rapid dynamic changes such as the polar cap, auroral zone, subauroral trough and equatorial anomaly. In addition, ionospheric models have not undergone as thorough validation as neutral atmosphere models simply because of the difficulty in measuring the ionospheric environment. Finally, the models require dynamical inputs that must be provided in a quasi-continuous fashion to enable accurate predictions.

4.2.3. AURORA

The aurora represents a bright and dynamic background with radiations from the ultraviolet through the long-wave infrared. Systems must acquire and track hostile targets at high latitudes and in the polar regions where aurora occur. For this reason, auroral modeling represents a crucial input for strategic scene generators. Unfortunately, investigators cannot appeal to any "standard" models of the aurora, as they can for the ionosphere and neutral atmosphere. However, several well-established "quasi-standards" do exist, and auroral and magnetospheric physicists often use these models to interpret their findings. One can divide auroral models into two principal types: models that deal with auroral morphology and models that deal with auroral emission intensities. So far, no single model incorporates both the intensity and the morphology of an aurora nor does one single model span all wavelengths from the infrared through the ultraviolet.

The auroral oval model of Feldstein (or Feldstein-Starkov) occupies the most prominent place among morphological models of the aurora. From observations of all-sky cameras during the International Geophysical Year, 1957-59, Feldstein constructed statistical maps of the probability of auroral occurrence for various levels of geomagnetic activity (e.g., Feldstein, 1963; Feldstein and Shevnina, 1963). The original versions of the Feldstein model related oval size and location to the 15 minute range index Q or Q_p, although later versions sometimes utilized the 3 hour K_p index (e.g., Feldstein, 1966). According to this statistical model, the oval remains fixed relative to the sun and the Earth rotates beneath it. When mapped in geomagnetic latitude and local time, the oval displays a day-night asymmetry (thinner on dayside, thicker on nightside), and, during times of geomagnetic activity as reflected in the Q or K indices, the oval tends to expand in area and move equatorward.

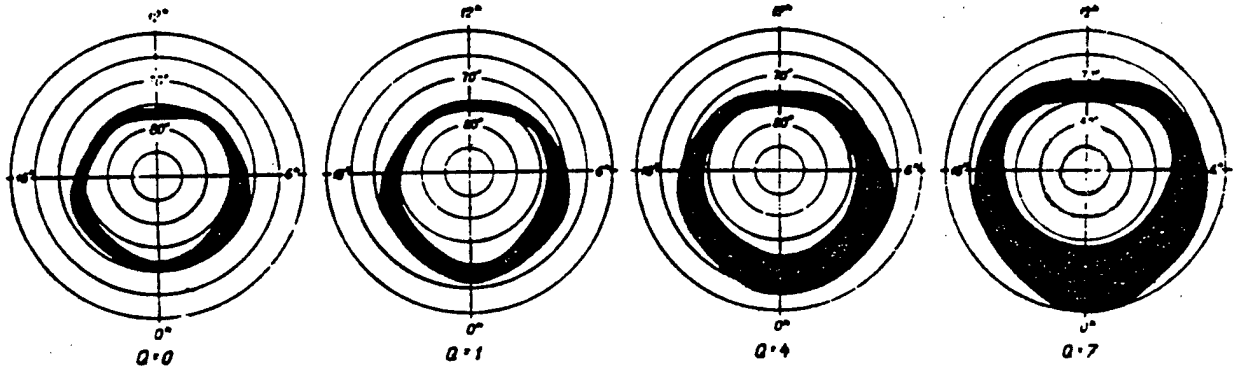

Fig. 4-3. The auroral oval at various geomagnetic activity levels (from Feldstein and Starkov, 1967; Feldstein and Galperin, 1985).

(see Fig. 4-3). The model sometimes appeared without specific equations, although the authors stated fitted curves in later versions (e.g., Feldstein, 1966; Feldstein and Starkov, 1967; Starkov, 1969). The Feldstein oval often appeared as either a contour map of occurrence probabilities (e.g., Feldstein, 1966) or as merely the 70% occurrence contours (e.g., Akasofu, 1968). The model and its various extensions are currently expressed in terms of fitted equations suitable for use by digital computer (Feldstein and Galperin, 1985). This "enhanced oval" model incorporates measurements from satellites as well as from the ground and expresses oval size and boundary position in terms of geomagnetic indices (K_p, AE, MLT) and interplanetary field components (B_y and B_z). For example, fitting data from DMSP photographs, Holzworth and Meng (1975) and later Holzworth (1984) portrayed the auroral oval as a circle offset from the geomagnetic pole. This empirical model related the center of the auroral circle and the circle's radius to the z component of the interplanetary magnetic field (B_z) rather than to any geomagnetic index such as K_p.

However, models of the statistically-defined oval do not readily address auroral dynamics, which are intimately related to those of the polar substorm and geomagnetic storm (e.g., Akasofu, 1968; Kamide, 1980). Although the behavior of the auroral oval is statistically defined during such disturbances, the individual auroral displays appear chaotic and unpredictable. Ground-based observations show that as a substorm progresses, certain auroral forms usually occur at certain local times along the oval and may even travel along the oval as a wave phenomena (e.g., Akasofu, 1964, 1965). The oval undergoes expansion and contraction at rates statistically related to the interplanetary magnetic field (e.g., Nakai et al., 1986). Furthermore, auroral arcs may also appear within the polar cap, not just along the oval (e.g., Eather and

Akasofu, 1969). Although statistical studies and qualitative models of auroral dynamics exist, no one has yet advanced a quantitative model can explain to explain the details of auroral dynamics. Figure 4-4 shows a schematic diagram of the principal morphological characteristics of the oval during a substorm.

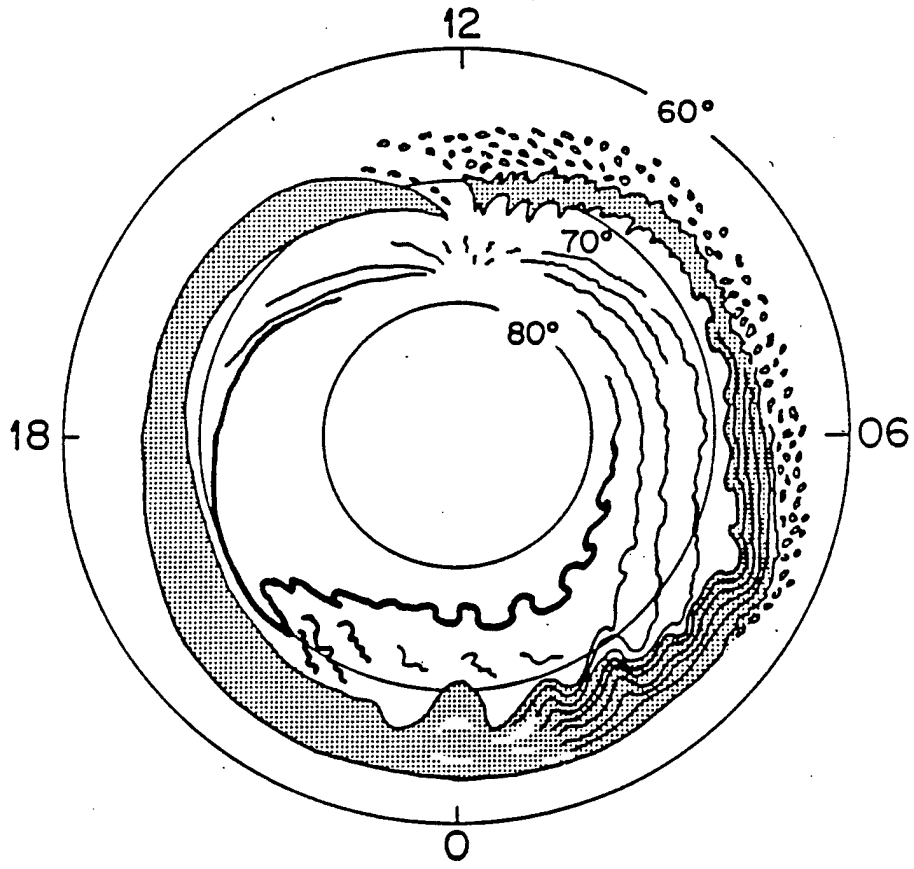

Fig. 4-4. Schematic diagram showing the main characteristics of auroras during an auroral substorm in dipole-MLT coordinates. Discrete arcs are indicated by lines and the diffuse auroral regions are shaded. (from Akasofu, 1976).

Global or near-global observations by polar orbiting spacecraft have verified the essential characteristics of the Feldstein oval and the Akasofu substorm models. The optical observations of the ISIS 2 satellite (e.g., Lui et al., 1975a,b), the DMSP satellite (e.g., Akasofu, 1974, 1976), and the DE-1 satellite (Frank et al., 1982) confirmed various morphological and dynamical aspects of aurora such as the continuity of the oval through 360° of longitude, the conjugacy of activity in the northern and southern auroral regions, and the oval's expansion and contraction in response to the interplanetary magnetic field. Figure 4-5 exhibits a near ultraviolet image of a portion of the

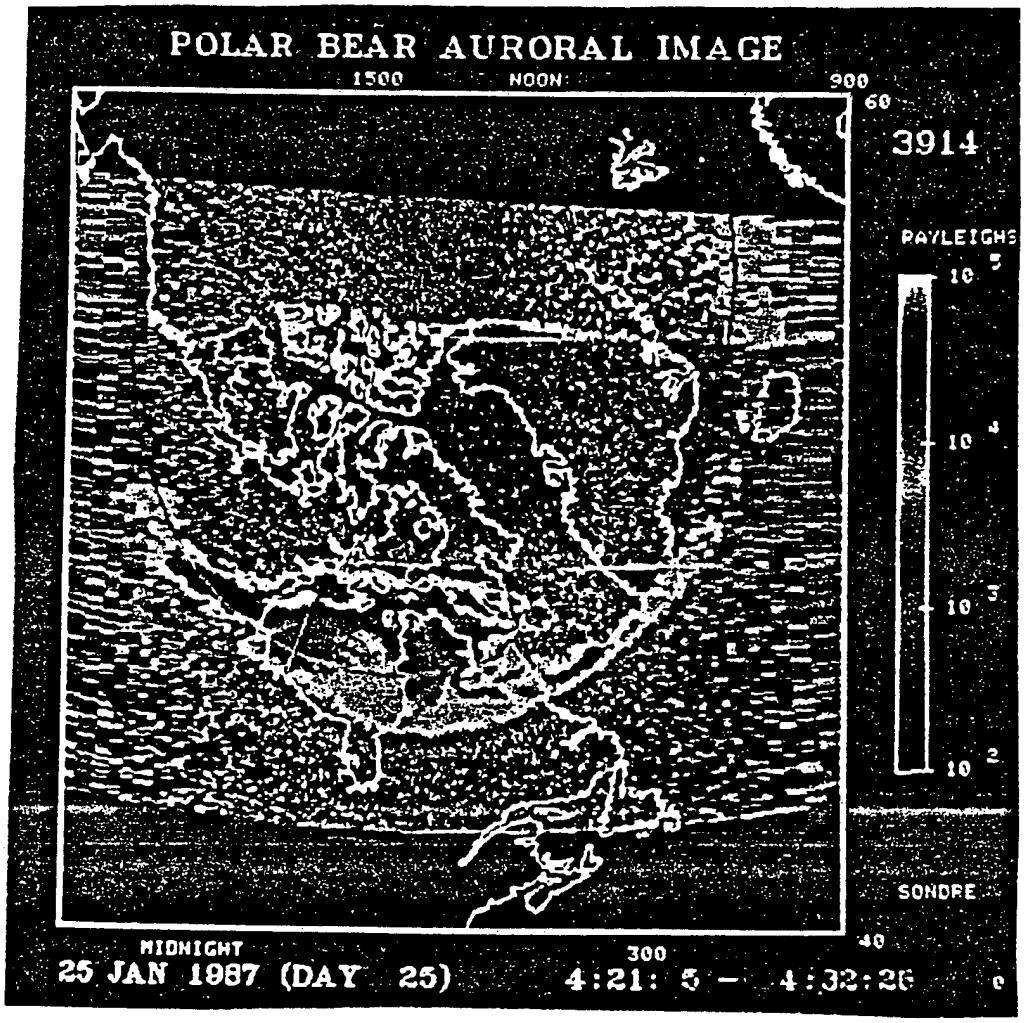

Fig. 4-5. The auroral oval during moderate substorm activity (AE~700 nT). The picture shows radiation from the N_2^+ (1N) emission.

auroral oval observed by a scanning photometer on the USAF Polar Bear satellite. Many of the features in this observation can be recognized in the qualitative model of Akasofu (Fig. 4-4).

Precipitating charged particles that actually cause the aurora may also serve to delineate the auroral and mark specific features. In the spirit of Feldstein's original work, satellite-based precipitation models also define auroral boundaries and features in terms of magnetic indices (K_p or AE) or the interplanetary magnetic field (B_z or B_y). For example, Kamide and Winningham (1977) and Gussenhoven et al. (1983) defined the oval's equatorward boundary based on precipitating electron data from the ISIS and DMSP satellites; Hardy et al. (1985) utilized electron data from the DMSP and STP P78-1 satellites to determine the average characteristics of auroral precipitation as a function of MLT, MLAT, and K_p. These empirical models incorporate not only the two-dimensional spatial morphology of aurora, but also the fluences and energies of the precipitating auroral electrons. Knowledge of the precipitating particle characteristics makes possible models

of auroral emission intensities, which constitute the second major type of auroral model— the emission intensity model.

In principal, one can calculate auroral emission intensities given a knowledge of the neutral atmosphere and the energy spectra and fluxes of precipitating particles. Current models of auroral emission processes employ calculational techniques outlined in standard auroral references such as Chamberlain (1961) or Vallance Jones (1974). Basically, the models assume a particle distribution (often a Maxwellian or Gaussian energy distribution), a neutral atmosphere (often the J77 or MSIS-86 model), and various interaction mechanisms; the models then compute the excitation and volume emission rates from atmospheric species impacted by the precipitating particles. The models also perform the inverse calculation: determining the precipitating particle flux and energy from the observed intensities, usually by taking intensity ratios of selected emissions (e.g., Rees and Luckey, 1974). A number of factors may render either type of calculation exceedingly complex and tenuous: disputed or unmeasured cross sections, indeterminate chemical reaction paths, effects of atmospheric turbulence and transport (a special problem for infrared auroral emissions), multiple scattering of emitted radiation, imperfect knowledge of the incident spectrum, and imperfect knowledge of the neutral atmosphere. For example, after a full century of scientific investigation, explanation of the prominent 557.7 nm auroral emission remains uncertain, especially at low altitudes (<250 km), largely because of chemical reaction paths, which number 17 in recent models (e.g., Sharp et al., 1983; Solomon et al., 1988).

Auroral emissions in the far ultraviolet (<300 nm) represent the most straightforward theoretical target for modeling. FUV emissions appear prominently in auroral spectrum and do not suffer from chemical dependences, wavelength blending problems, or background albedo confusion (e.g., Strickland et al., 1983). FUV models do require that electron transport calculations be performed, but this calculation seems well understood (Strickland et al., 1976). Because of their sensitivity to precipitating particles, current models of FUV auroral emissions derive characteristic energies and fluxes of precipitating electrons given the observed emissions (e.g., Strickland et al., 1989a). This calculation could, however, be inverted so that FUV emissions may be calculated given the flux and spectrum of precipitating particles.

Auroral emissions in the infrared (>2 μm) are more difficult to model because they require knowledge of the history of energy deposited during the aurora (e.g., Ulwick et al., 1985; Robertson et al., 1988). For instance, a slow drizzle of electrons over a long period of time can enhance the 4.3 μm CO_2 radiance. Atmospheric winds can carry vibrationally-excited N_2 to great distances outside the oval, where it can collide with CO_2 and give rise to 4.3 μm emission. Processes such as Joule heating, self-absorption, and radiative transport can also produce infrared emissions well away from the region of electron energy deposition. Because of these effects, the mere measurement

of radiance does not offer an adequate description nor suffice to predict the intensity and phenomenology of infrared aurora.

The Auroral Atmospheric Radiance Code (AARC), under development by the Geophysics Laboratory, attempts to overcome these difficulties by predicting auroral radiation in the 2 μm to 7 μm region (Winick et al., 1987). AARC accepts a model atmosphere (USSA is default) and assumes the uniform deposition of electrons within an auroral arc. The model then computes emissions resulting from the chemiluminescence of H_2O (2.7 μm), NO (3.0 and 5.3 μm), and CO_2 (4.3 μm). AARC includes chemistry, photon emission, and radiative transfer following the electron deposition. Assuming the appropriate auroral dosing data are acquired, future versions of AARC will extend this coverage to the long wavelength infrared. Figure 4-6 shows and example of AARC calculations for IBC II and IBC III auroral conditions.

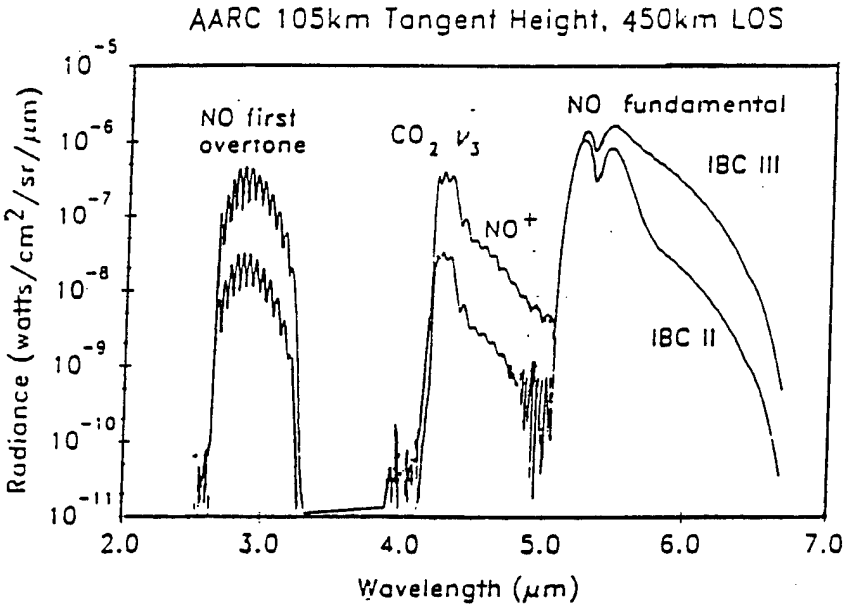

Fig. 4-6. IR radiances predicted by the AARC model for IBC II and III auroral conditions.

Auroral models suffer from a number of deficiencies. First, the models have limited scales of validity. Global models of the auroral oval and its dynamics cannot describe the small-scale effects realized in the vicinity of auroral arcs or boundary regions. Indeed, such local effects have a probabilistic nature that mitigates against their deterministic prediction. Second, the models require inputs provided only by a large and expensive network of observing stations. These input parameters include solar wind speed, pressure, density, and the interplanetary magnetic field (obtained from high Earth orbit); magnetic indices such as AE, AL, or AU (obtained from an array of ground magnetometers); thermospheric and mesospheric dynamics (obtained from ground radar or lidar sounders). Third, the models have not

undergone a complete validation and, indeed, often inspire rather spirited scientific debates as to their reliability and applicability. Fourth, the models may not have user-friendly interfaces and can be accessed only through special arrangements with the proprietary authors. AARC attempts to remedy this situation, although short wavelength codes have a reputation of proprietary control. Fifth, the complex nature of the IR models presents a number of uncertainties. These include ozone fluorescence, N_2O formation, Joule heating, and chemical-dynamical processes in general. Finally, no single auroral model incorporates ultraviolet, visible and infrared radiations, and no single platform has simultaneously observed radiations in all three regimes. MSX represents the first attempt to measure, from an orbital platform, the totality of auroral radiations and obtain a comprehensive picture of the aurora.

4.2.4. ATMOSPHERIC EARTHLIMB EMISSIONS

Investigation of Earth limb radiances represents a central theme of MSX background measurements. In particular, the terrestrial backgrounds team will evaluate two atmospheric infrared emission codes for estimating the radiance of the Earthlimb. The High Altitude Infrared Radiance Model (HAIRM) predicts the radiance from a quiescent atmosphere for lines of sight above 60 km (Degges and Smith, 1977; Sharma et al., 1987). HAIRM includes Earth shine, collisional interactions of atmospheric species, and uses a band model approach. The Strategic High Altitude Radiance Code (SHARC) predicts the quiescent Earth limb radiance from 2 to 25 μm between altitudes of 50 to 300 km (e.g., Sharma et al., 1989). SHARC uses a non-LTE approach because the vibrational temperature of atmospheric species becomes decoupled from the kinetic temperature at altitudes above 60 km. The model also takes into account Earth shine and solar pumping.

These output of these two models has been used to interpret observations of the infrared limb. HAIRM and SHARC reproduced the total band intensities of the most prominent features observed by the SPIRE experiment, a rocket-based survey of limb emissions in both day and night atmospheres (Stair, 1985). The SPIRE observations have permitted the revision of HAIRM to include infrared radiative processes identified in the database, which SHARC also uses. The models calculation of the peak radiance and total band intensities agree well with the SPIRE data. HAIRM has recently predicted the O_3 emissions observed by the SPIRIT I detector during an IBC III aurora (Robertson et al., 1988; Alder-Golden, 1990). Both the model and the data revealed the so-called "hot-band" spectral structure considered a crucial test of the model and the instrument (Fig. 4-7).

Although HAIRM and SHARC have enjoyed success in comparison with SPIRE data, the two models suffer from several deficiencies. First, the models do not satisfactorily predict spectral shapes. This problem could be caused by limited resolution of the band model calculation, by an insufficient number of highly excited vibrational states, or by lack of all pertinent radiators. Second, the models lack an accurate estimate of H_2O concentration

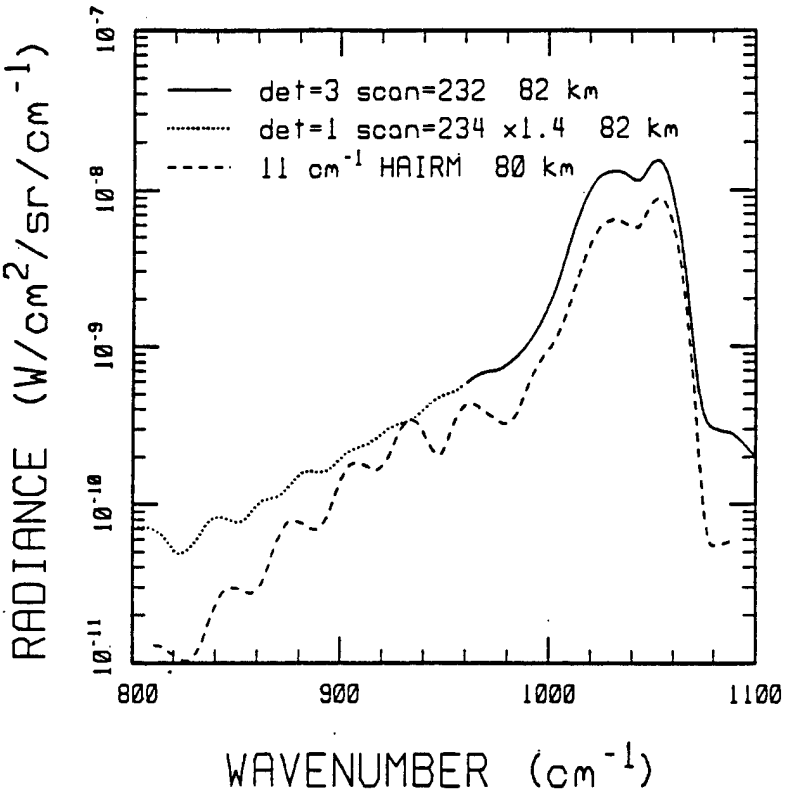

Fig. 4-7. Comparison of SPIRIT I and HAIRM model ozone spectra near 80 km tangent height (from Alder-Golden et al., 1990).

at ~100 km altitude. Although a trace constituent, water is the dominant emitter in the 17-25 μm region at such altitudes and exhibits extreme and unpredictable variations (Olivero, 1986). Third, model predictions in the 6-9 μm and 11-13 μm regions suffer because not all radiative species nor processes are known and the model has not been fully validated. Fourth, the two models include uncertainties in local kinetic and vibrational temperatures, quenching rates, and dynamical behavior of the upper atmosphere. The models especially require high altitude information on the concentrations and movements of minor species such as NO (5.3 μm), O_3 (9.6 μm), and CO_2 (15 μm), all of which contribute significantly to the limb infrared emissions.

4.2.5. ATMOSPHERIC RADIANCE AND TRANSMITTANCE

Most radiation emerges from the atmosphere as a consequence of solar radiation backscattered from atmospheric molecules and aerosols (or particulates). Originating with Lord Rayleigh (Strutt, 1871), the theory of molecular scattering offers a rather complete and successful description of the intensity and polarization of radiation backscattered by atmospheric gases. Modern computers have made the Rayleigh scattering theory easily accessible, either in tabular form (e.g., Coulson et al., 1959a,b) or in the form of a computer algorithm that can be incorporated into radiation codes (e.g., Strickland et al., 1989b).

Scattering by aerosols, however, represents a formidable problem that has consumed considerable theoretical effort. Consequently, the original Mie theory has been extended from single scattering to multiple scattering by the use of various analytical and numerical artifices (e.g., Hansen and Travis, 1974; van de Hulst, 1980). Modern computer codes such as LOWTRAN include some of the effects of particulate scattering in a statistical sense, although they usually do not perform a full numerical computation.

Typical codes model atmospheric radiation based on processes such as transmission, refraction, attenuation, and atomic and molecular emissions. The standard models, developed and maintained by the Geophysics Laboratory, generally apply to radiation at visible and longer wavelengths. The codes include three principal models: the Fast Atmospheric Signature Code (FASCODE), the Moderate Resolution Transmittance Code (MODTRAN), and the Low Resolution Transmittance Code (LOWTRAN). Although differing in spectral resolution and absorption-emission methodologies, these three codes incorporate a set of common elements and use the standard spectroscopic parameters of the High Resolution Transmission Code (HITRAN) (Rothman et al., 1986).

The most commonly used of the three models is the semi-empirical LOWTRAN (Kneizys et al., 1988). Using molecular band methods, this model calculates the attenuation of a beam penetrating the atmosphere at various geometries and under various atmospheric conditions. The model includes the effects of Rayleigh and Mie scattering, atmospheric refraction, surface albedo, and, to some extent, climate. Within LOWTRAN, users can select from six atmospheric profiles, seven aerosol models, two fog models, and several cloud models. The most recent version of LOWTRAN covers the wavelength regime from 0.2 μm to 25 μm with a spectral resolution of ~5 Å (20 cm^{-1}) and is useful from the surface up to ~120 km. LOWTRAN utilizes climatologically-varying profiles for minor species such as H_2O, O_3, CH_4, CO, and NO_2; these profiles originate from standard atmospheric models such as CIRA and USSA, or can be supplied directly by the user. LOWTRAN represents the collective efforts of numerous authors who developed the model over 20 years. Version 7 has recently been released and is available on small personal computers. Many workers rely on LOWTRAN, which has undergone extensive validation.

FASCODE and MODTRAN perform essentially the same tasks as LOWTRAN. FASCODE represents an "exact", highly-optimized, line-by-line code that includes both LTE and NLTE radiative transfer (Clough et al., 1987, 1989). Like LOWTRAN, MODCODE uses a distinct band-model parameterization method (reference). MODCODE has a moderately high resolution of 2 cm^{-1}, an order of magnitude finer than LOWTRAN.

All three codes all utilize input from HITRAN, which determines atmospheric emission and absorption using both laboratory measurements and atomic theory (Rothman et al., 1986). HITRAN includes rotation, vibration, and electronic transitions for the molecules in its database. The model represents ~500,000 lines of optimized computer code. HITRAN boasts

an extremely high spectral resolution exceeding 0.1Å. Unfortunately, users must go through considerable gyrations to access the program.

The wide use of these codes, especially LOWTRAN, suggests that the models have undergone a wholesome validation. Nonetheless, the models have several deficiencies worth noting. First, such codes produce only a statistical average picture and will not produce the "fine-structure" fluctuations observed in actual measurements of atmospheric radiance. For example, they neglect small-scale waves that can significantly affect the limb radiance structures. Second, the models are weighted heavily toward the visible and long wavelength regimes and have not undergone complete validation below ~0.30 μm. The models are continually evolving. Newer versions will include improved climatologies as a result of upgrades in the CIRA input model.

4.2.6. ATMOSPHERIC DYNAMICS

The atmosphere displays complex motions ranging in size from global-scale circulations to turbulence only a few centimeters in size and durations as long as months or as brief as seconds. Atmospheric radiance exhibits structures and histories that correspond closely to these motions, which must be incorporated into background models. The MSX mission will focus on the dynamical processes that transport energy and alter temperature and composition of the middle and upper atmosphere (z>60 km).

Atmospheric waves represent phenomena of particular interest to the MSX mission. Such waves transport energy and momentum and alter the mean zonal flows in the atmosphere. Table 4-2 summarizes the principal categories of atmospheric waves and indicates their scale sizes and sources. Planetary waves can give rise to moderate cooling rates (~5 K/day) in the mid-latitudes and strong heating rates (~10-20 K/day) at high latitudes (Geller, 1984) but usually do not produce effects in the thermosphere (e.g., Charney and Drazin, 1961; Hooke, 1983). Tides, however, can efficiently propagate their energy vertically and produce substantial energy fluxes at thermospheric heights (Lindzen and Blake, 1970). Operating on smaller scales, gravity waves propagate from the lower atmosphere to the middle and upper atmospheres and release energy through turbulent "breaking" (e.g., Hines, 1974; Lindzen, 1981). Both tides and gravity waves can have pronounced effects on the zonal circulation of the middle and upper atmospheres (Lindzen, 1981). Gravity wave breaking can produce other effects such as the heat transport, wave scattering, induced drag, and turbulent diffusion (e.g., Fritts, 1984). One chemical-dynamic model of indicates that gravity waves can strongly affect the O_3 and OH concentrations at the nightside mesopause (Walterscheid and Schubert (1989).

The observation of atmospheric waves has utilized numerous experimental techniques. Traditionally, instruments on balloons and rockets and ground sightings of meteor trails and noctilucent clouds have served to directly measure motions of the middle and upper atmosphere (e.g., Gage and Van Zandt (1981). However, modern techniques using ground radar and pro-

Table 4-2
ATMOSPHERIC WAVES (from Hooke, 1977; Fritts, 1984)

wave	λ	τ	v_{phase}	motion	source
Rossby—planetary	~R_E (hor)	~5T_E	$<<\frac{R_E}{T_E}$	geostroph. hydrostatic	instability topo. feature differential heating
Tides	$\frac{\sim 2\pi R_E}{n}$ n=1,2...	$\frac{\sim T_E}{n}$ n=1,2...	$\frac{\sim 2\pi R_E}{T_E}$	non-geostr. hydrostatic	solar/lunar gravity solar heating
Gravity	10^0-10^3 km (hor) 1-20 km (ver)	$<<T_E$	$<C_o$	non-geostr. non-hydrostat.	instability topo. feature differential heating wave-wave interac.

where R_E= Earth radius, T_E= solar day, $2\pi R_E/T_E$=460 m/sec, C_o=sound speed

vide extended measurements of upper atmospheric parameters such as density, speed, and temperature (e.g., Manson et al., 1981; Balsley and Carter, 1982; Chanin and Hauchecorne, 1981). The analyses of observations of atmospheric dynamics often employ power-spectra analyses of the wave measurements (e.g., Balsley and Carter, 1982; Van Zandt 1982; Philbrick et al., 1983). This technique has special utility for clutter analysis (see Section 4.2.6).

Because of their potential impact on the temperatures of the upper atmosphere, stratospheric warmings represent a special class of atmospheric phenomena requiring attention by MSX. The warmings represent temperature changes of 40-60K over the space of a few days (e.g., Holton, 1972; Schoeberl, 1978). Stratospheric warmings occur sporadically and disruptively in the northern winter at latitudes above 60° north (Labitzke, 1980). The warmings penetrate the upper mesosphere (60-70 km) as well as the stratosphere and can distort or completely disrupt the zonal circulation of the polar vortex (e.g. Labitzke, 1981). Matsuno (1971) proposed that the interaction of the zonally averaged circulation with planetary waves produced stratospheric warmings, and later numerical models essentially confirmed this approach (e.g., Holton, 1976). Recent numerical models have used a so-called transformed Eulerian-mean approach and suggest that a major warming requires "preconditioning" of zonal flow by an earlier warming pulse (e.g., Dunkerton et al., 1981; Palmer, 1981). Forecasting of

stratospheric warmings have been conducted with some success by Butchart et al. (1982) and Simmons and Strüfing (1982) but has not attained an advanced (or reliable) state.

Atmospheric dynamics models also include general circulation models (GCMs), which attempt to numerically solve the "primitive" fluid dynamic equations of motion. High-speed computers have rendered this type of modeling increasingly productive. In the middle atmosphere, three principal types of circulation models exist. The NOAA Geophysical Fluid Dynamics Laboratory (GFDL) model is the most comprehensive of these. The GFDL model has 40 vertical levels extending to 80 km and includes full radiative transfer, topography, a hydrological cycle, surface boundary processes, and a realistic Richardson number (e.g., Geller, 1982). Mechanistic circulation models such as the NASA Langley Research Center (LRC) model include topography, simple radiative transfer, and specify tropospheric forcing by an empirical formulation (e.g., Cunnold et al., 1975). A third class of models, the mechanistic models, rely on forcings specified at the lower boundary; the forcings may include radiative heating or gravity wave turbulence (e.g., Holton and Wehrbein, 1980; Schoeberl and Strobel, 1978).

Computer models of thermospheric circulation usually bear the appellation of Thermospheric General Circulation Models (TGCMs) or Ionospheric General Circulation Models (IGCMs), depending on the emphasis of the model. The two leading TGCMs originated at the National Center for Atmospheric Research (the NCAR-TGCM) and the University College of London (the UCL-TGCM). The models perform massive 3D, time-dependent numerical calculations that solve the primitive equations of lower-atmospheric dynamic meteorology on a global basis (Fuller-Rowell and Rees, 1980; Dickinson et al., 1981). Typically, such models require as input a neutral atmosphere model (such as MSIS), a representation of solar radiation, a high latitude heat source (such as precipitating electrons), and an ion-drag forcing function (e.g., Dickinson et al., 1981). From their inception in the early 1980's, the models have evolved to include more effects and more realistic boundary conditions. Thermospheric composition, the coupling of the thermosphere to the ionosphere, and the inclusion of tides represent important effects incorporated in current versions of the NCAR and UCL models (Fuller-Rowell and Rees, 1983, 1987; Dickinson et al., 1984; Fesen et al., 1986). The models are valid from ~100 km to the exopause (~500-700 km).

The TGCM models have undergone validation in two ways. First, the models can be compared to the generally observed or expected behavior of the thermosphere. For example, Fuller-Rowell and Rees (1981) simulated the response of the thermosphere to a model of a geomagnetic substorm rather than relying on the inchoate data from disparate observational systems. Second, the models can be compared directly to measurements taken during a specific geodynamical event such as a geomagnetic storm. Initially, such comparisons involved the use of a limited dataset from rockets or ground measurements (e.g., Rees et al., 1980) or of a statistically-averaged model such as MSIS (e.g., Dickinson et al., 1984). In such cases, the modelers could usually

produce agreement by cleverly adjusting input parameters (e.g., Killeen, 1987). However, the massive databases available from coordinated investigations such as the Coordinated Data Analysis Workshops (CDAWs) and the Equinox Transition Study (ETS) have provided modelers with much more tightly constrained inputs. In such cases, TGCMs may disagree substantially with observations. For example, the NCAR-TGCM produced excessive exospheric temperatures and incorrect wind reversals when compared to observations from CDAW6 (Roble et al., 1987; Forbes et al., 1987).

Two other types of dynamical thermosphere models appear in the literature. The transfer function model (TFM) describes the global thermospheric response to time dependent sources (Mayr et al., 1984a,b), while other types of models describe the local dynamics associated with small scale thermospheric events such as auroral arcs (e.g., Walterscheid et al., 1985). The TFM treats acoustic gravity waves as perturbations of a globally uniform atmosphere and determines the resulting wave distribution. Local dynamical models represent attempts to model the thermosphere on the more intimate scales of auroral arcs and boundary features; the models have begun to utilize observational data as inputs (e.g., Walterscheid and Lyons, 1989) but have yet to undergo the extensive scrutiny of the global models.

4.2.7. ATMOSPHERIC CLUTTER

The spatial and temporal variations of the atmospheric radiation represent background clutter, which concerns all space surveillance and tracking systems. These systems must detect small-scale targets such as plumes and re-entry vehicles against limb backgrounds that may present spatial and temporal variations of comparable scales and intensities (e.g., Ratkowski et al., 1986). The performance of these systems against such backgrounds may be measured in terms of a Probability of Detection (PD) and False Alarm Rate (FAR) (e.g. Simons, 1974). A spatial or temporal Fourier transform of the observed scene produces a power spectral density (PSD) that quantifies the clutter in terms of a power spectral index, "break point" wavelength or wave number, and structure amplitude. That is, $PSD \approx A(f/f_0)^{-n}$, where f is frequency (either spatial or temporal), A is amplitude, and n is spectral index. Figure 4-8 illustrates a model PSD from which power spectral index (n_1 and n_2) and correlation lengths (L_1 and L_2) can be obtained directly from fitting the PSD curve. Such quantities can, in turn, be directly incorporated into estimates of target signal-to-noise ratios for direct use by system planners (e.g., Malkmus et al., 1989).

Atmospheric clutter is intimately related to atmospheric structure and dynamics. In particular, measurements by ground-based radars and ladars can quantify atmospheric wave activity in terms of power spectral densities similar to those of scene radiance. A number of such PSD analyses have determined wavelengths and periods of waves in the middle and upper atmosphere (e.g., Watkins and Wand, 1981; Chanin and Hauchecorne, 1981; Balsley and Carter, 1982). Using data from several observations, Van Zandt (1982) suggested that buoyancy waves have a common spectral form and pro-

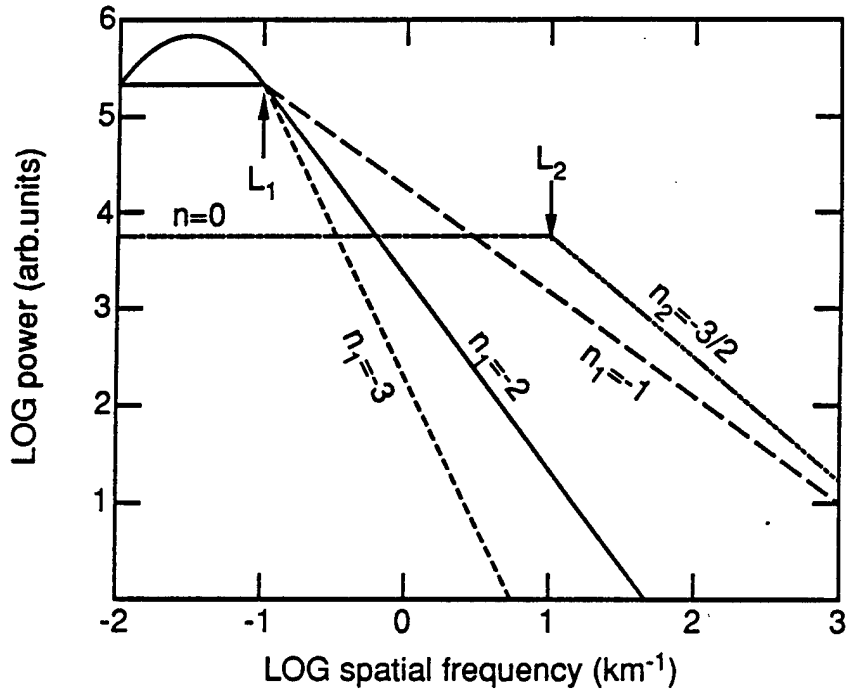

Fig. 4-8. Model of Power Spectral Density for limb clutter.

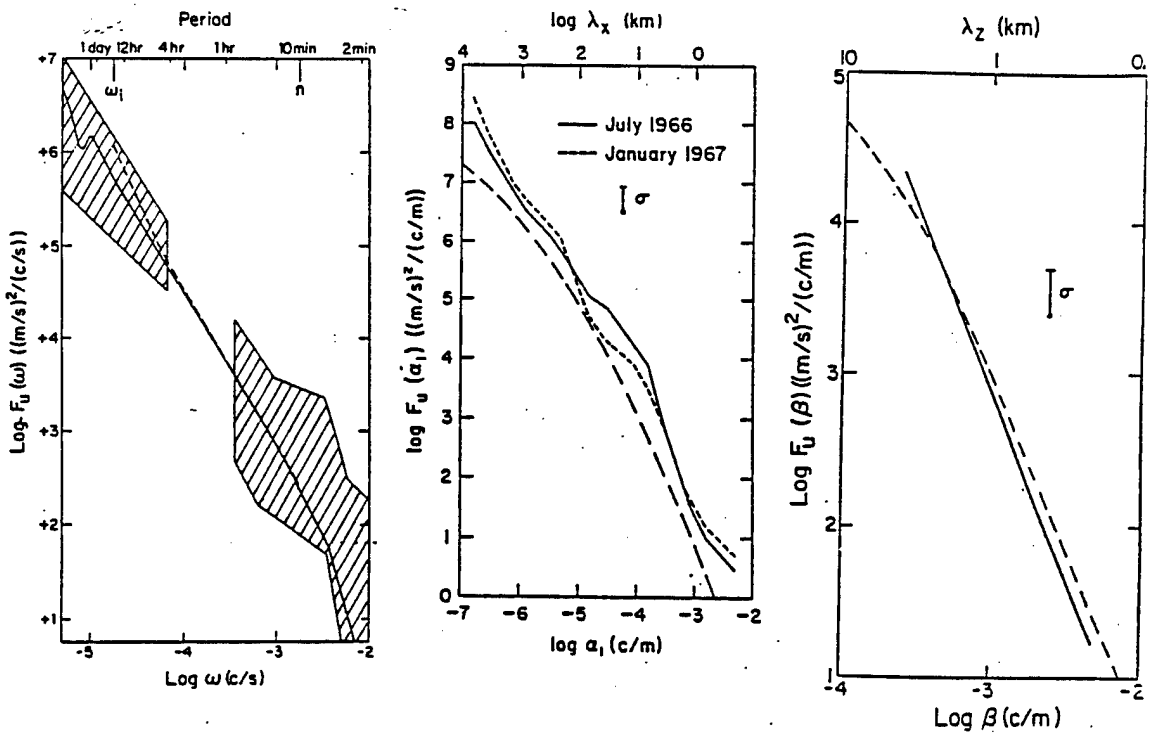

Fig. 4-9. Power spectral densities for "universal waves." Shown left to right are horizontal wind PSDs in frequency, in horizontal wave number and in vertical wave number. (from Van Zandt, 1982)

posed "universal" PSDs for temporal, horizontal, and vertical waves. Figure 4-9 illustrates the similarity of these PSDs to the model PSD of Fig. 4-8. Measurement of the wave PSD therefore effectively determines the scene PSD and provides an indirect estimate of the scene clutter caused by the atmospheric background.

Although virtually any observation of the terrestrial background scene could provide clutter information, surprisingly few investigations have directly measured the clutter of atmospheric background radiance. Infrared radiance analyses are limited to those of the ELIAS, ELC, and MAPSTAR experiments. The ELIAS program measured the spatial structure of the aurora and airglow in the SWIR and MWIR and demonstrated that aurora are highly structured (Nadile, 1984). The ELC program measured the quiescent Earth limb radiance in various LWIR bands and discovered structure with a ~2.5 km footprint in the background. Sponsored by AFSOR, MAPSTAR measures and models the structure of the terrestrial airglow. To date, however, there exists no direct clutter measurement of the upper atmosphere in the LWIR.

Several investigations of background clutter have been carried out for ultraviolet and visible radiance. Indeed, a considerable number of workers have examined the brightness fluctuations of ultraviolet and visible auroral emissions. Power spectral analyses of fluctuations in common auroral emissions (OI at 0.5577 μm and N_2^+ at 0.3914 μm) evidenced peaks at 3 Hz and 10 Hz and are though to be related to bunches of precipitating electrons (Pemberton and Shepherd, 1975). A fractal investigation using imager data from the Polar Bear satellite suggested that the spatial structures of the OI 0.1304 μm background were controlled principally by turbulence over scales of 10^2-10^7 m and modified by Rayleigh scattering and magnetospheric forcing (Huguenin et al., 1989; Wohlers et al., 1989). Malkmus et al. (1989) constructed a limb clutter model for the middle ultraviolet (0.2-0.3 μm) and the visible (0.4-0.7 μm) and, assuming a target radiant intensity, derived signal to noise ratios (Fig. 4-10). Recently, Ross (1990) used Delta 181 limb images to determine background clutter caused by nighttime O_2 Herzberg I emissions (0.26-0.30 μm). This investigation obtained evidence for the direct observation of gravity waves from the structure in the Herzberg I emissions. These several attempts at determining the UV-visible clutter indicate that the clutter will be different at different wavelengths and that monochromatic measurements will probably yield inaccurate clutter estimates.

Models of the background clutter suffer dramatically from a lack of direct measurements at virtually all wavelengths. Most estimates of clutter rely on measurements of atmospheric structures made, for example, by ground radars and ladars. Even these ground-based measurements represent single-point measurements having inappropriate space and time resolution, improper observation geometries, and poor coverage. Geomagnetic activity may drastically affect atmospheric structure, and its affect on scene clutter must also be investigated.

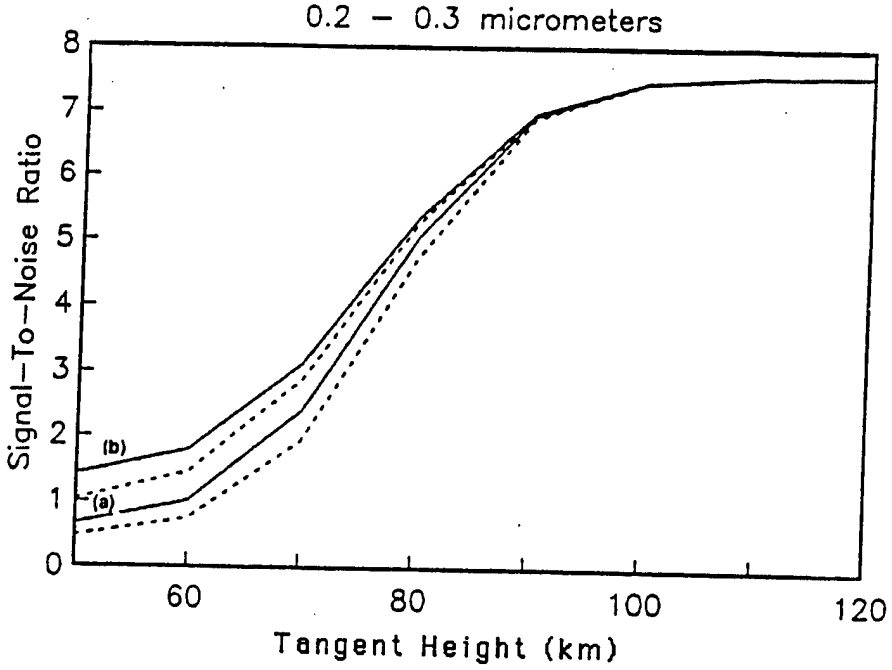

Fig. 4-10. SNR calculations using the clutter UV limb clutter (Malkmus et al., 1989). Dashed lines show the effect of varying clutter by 50%.

4.2.8. ATMOSPHERIC AIRGLOW EMISSIONS

Airglow represents the amorphous, optical radiation continuously emitted by the Earth's atmosphere and extending in wavelength from the extreme ultraviolet (<0.100 μm) to the infrared (>1.00 μm) (e.g., Chamberlain, 1978). Airglow arises from the direct scattering of sunlight, from the creation or destruction of the ionosphere, or from the photochemistry of neutral constituents. Depending on the wavelength and atmospheric state, airglow may exist as a spatially diffuse emission or originate within a small layer having sharp azimuthal boundaries. Models of airglow usually explain individual measurements of intensity and spectra within a restricted wavelength regime and concentrate on only a few specific emissions. The models rely on a knowledge of the incident solar radiation, the atmosphere, and various interaction mechanisms. In some instances, a model may do no more than perform a simple inversion of backscattered radiation (e.g., Barth, 1964), while in other cases the model must include complicated atmospheric chemistry and electron transport (e.g., Conway and Christensen, 1985; Meier et al., 1985). In many cases, the complications involved in these calculations render even well-known airglow emissions incompletely understood (e.g., Bates, 1988). Recent model efforts have combined the Rayleigh and aerosol-

scattered backgrounds with models of thermospheric airglow to reproduce the full spectrum observed in the far and near ultraviolet (Anderson and Strickland, 1988; Strickland et al., 1989b). The extension of this model to the infrared, to high latitudes, and to the nightside promises the first comprehensive model of terrestrial airglow emissions.

4.2.9. POLAR MESOSPHERIC CLOUDS

At altitudes of ~83-85 km, polar mesospheric clouds (PMC) (and their ground-observed counterparts, noctilucent clouds (NLC)) represent bright backgrounds of several kR that persist for several weeks near the summer solstice (e.g., Gadsden, 1982; Thomas, 1984). The clouds may produce signatures much brighter than targets and might confuse sensors viewing the cooler atmospheric backgrounds. No model exists for the morphology of these clouds, although their altitudinal, seasonal, and latitudinal distributions are fairly well substantiated (e.g., Fogle and Haurwitz, 1966; Thomas and Olivero, 1989). Microphysical models of the clouds indicate they consist of ice particles formed from the deposition of water vapor in the cold, summertime mesopause (e.g., Turco et al., 1982). NLC and PMC apparently originate from the upwelling of water vapor carried by gravity waves (e.g., Garcia, 1989), although such upwelling may not be so important if recent summer mesopause temperatures are correct (von Zahn and Meyer, 1989). These clouds are far from understood, however, and investigators have not yet established whether NLC and PMC even represent the same phenomenon (e.g., Jensen et al., 1989).

4.3. REQUIRED MSX MEASUREMENTS

4.3.1. MISSION PHASES

The Earth backgrounds measurements may be divided into three principal phases: mini-mission, cryogen phase, and post-cryogen phase. These phases are ordered progressively in time.

During the mini-mission, which may last several weeks, the terrestrial observations encompass an initial survey of the Earth limb and auroral background scenes. The mini-mission will permit the initial start-up and check-out of the spacecraft and the instruments. Mini-mission observations will fully exercise the MSX instruments by including day and nighttime scenes of the upper atmosphere above ~60 km. Prior to the mini-mission, a "pre-cryogen phase" of a few days' duration may allow brief scans of the Earth surface by UVISI.

The cryogen phase of the mission will last until the SPIRIT instrument loses cryogen, which is estimated to last about two years. During this phase of the mission, the MSX instruments will observe the Earth limb backgrounds at tangent altitudes above ~60 km. Observations will include altitude scans, terminator crossings, auroral bright spots, polar mesospheric clouds, and atmospheric wave phenomena. These observations will permit the compilation of an extensive observational database of emissions of the middle and upper atmosphere.

After the SPIRIT cryogen is depleted, the shortwave instruments will extend MSX observations below tangent altitudes of 60 km to include the stratosphere, troposphere, and hard Earth. In these low-altitude regimes, solar backscattering dominates the radiation and presents a fundamentally different scene. Observations during the post-cryogen phase include nadir-looking views of auroral activity, ozone layer effects, and tropospheric weather. Additionally, the UVISI and SBV instruments will continue making measurements of the middle and upper atmospheres.

4.3.2. EARTH LIMB SEGMENTATION

Observations of the Earth limb will constitute the principal part of the backgrounds measurements made during the MSX mission. One may categorize Earth limb measurements in one of several ways. The Earth limb measurements may be divided into two categories based on altitude: the "high" limb (h>60 km) and the "low" limb (h<60 km). Earth limb observations could also be divided by solar zenith angle into day (0°-90°), twilight (90°-110°), and night (110°-180°). Finally, Earth limb observations can be categorized by orbital segments: low or equatorial latitudes (30°S-30°N), mid-latitudes (30°-60°), and high or polar latitudes (60°-90°). Figure 4-11 indicates the categorization of Earth limb measurements based on these subdivisions, while Fig. 4-12 illustrates the orbital segments. For the nominal 101 minute orbital period, the polar and low-latitude segments require 16.8 minutes to traverse, while the mid-latitude segments require 8.4 minutes. To conserve spacecraft resources, the Earth limb observations may be broken down into segments that need not be successively sampled. From an SDI

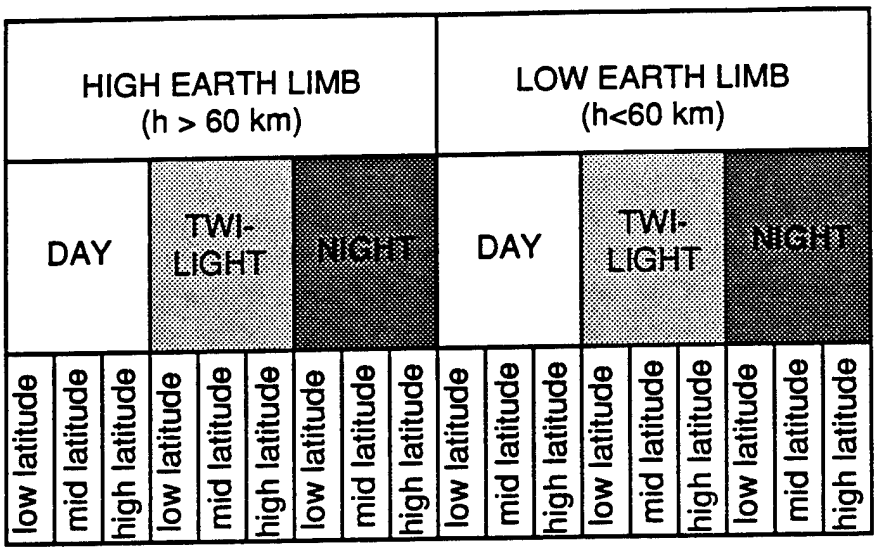

Fig. 4-11. Categorization of Earth limb measurements.

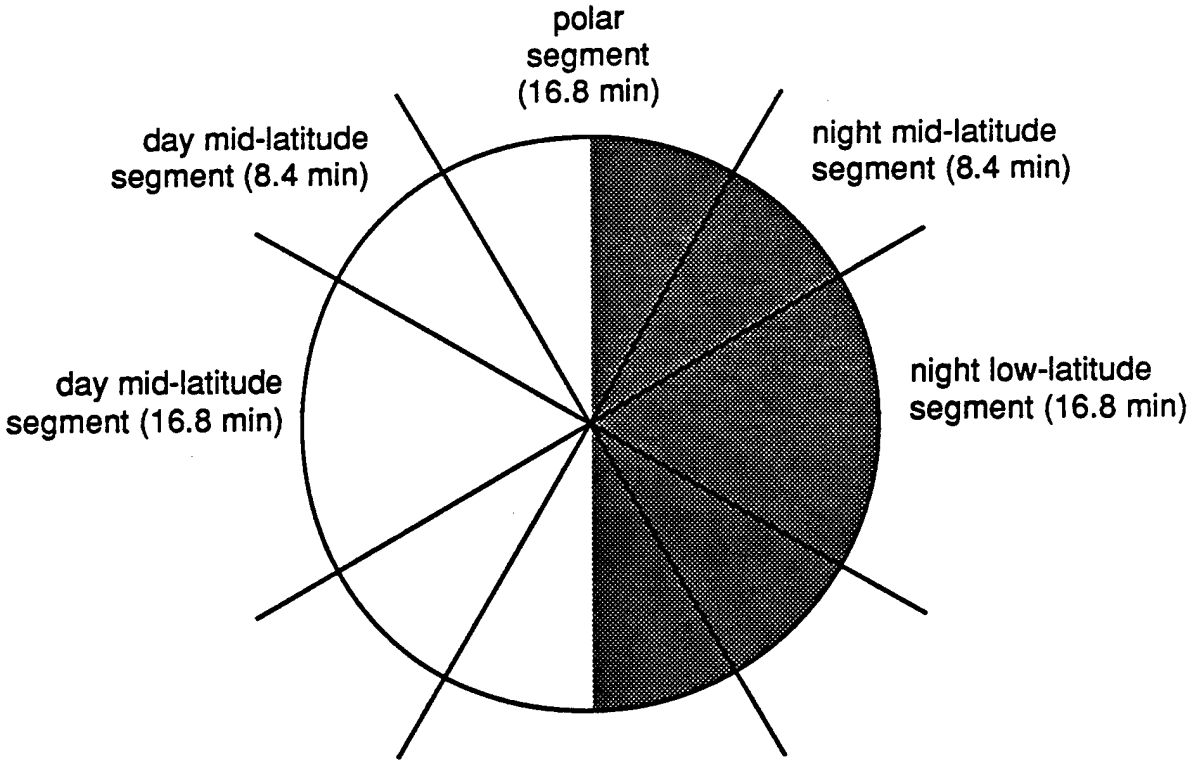

Fig. 4-12. Orbit segmentation for Earth limb observations. Each segment is 8.4 minutes long or 2x8.4= 16.8 minutes.

standpoint, the polar segment observations would have the highest priority, the mid-latitudes would have secondary priority, and the equatorial latitudes would be least important.

4.3.3. EARTH LIMB SCAN GEOMETRIES

During the cryogen phase of the mission, the instruments will view the limb at a grazing incidence that permits generation of altitude profiles. Figure 4-13 illustrates the basic viewing geometry contemplated for Earth limb observations. Quite simply, the MSX platform holds its attitude at a constant zenith angle declination so that the instruments sample a constant range of altitudes. A scene is generated in one of three ways: by the sweeping of the satellite's motion (SPIRIT not scanning), by rotating the satellite about its zenith axis ("coolie-hat" scan, SPIRIT not scanning), or by pointing the MSX centerline at a fixed latitude and longitude (SPIRIT scanning). The tangent altitude is chosen to select a phenomenon of interest. For example, polar mesospheric cloud investigations might select an 80 km tangent altitude, while auroral investigations might select a tangent altitude of 150 km, while geocorona investigations would select a tangent altitude of 500 km.

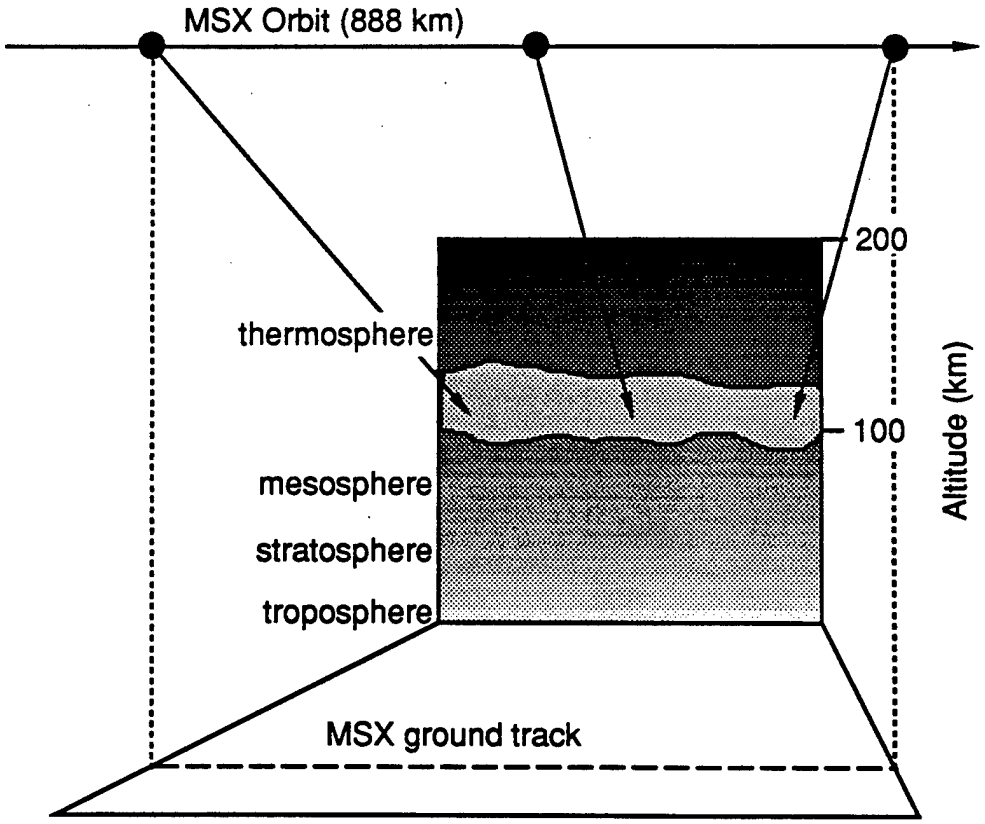

Fig. 4-13. Basic Earth limb viewing for MSX. The SPIRIT III boresight points at a constant tangent altitude. Shown here, the altitude corresponds to that of the bottom of the visible aurora. (A "flat Earth" is assumed.)

Limb-observation scenarios must take into account the differing fields of view of the instruments. Figure 4-14 compares the fields of view of the several instruments as they appear projected at various tangent altitudes. The SPIRIT and UVISI/SPIM fields of regard represent fields swept by scan mirrors, while the UVISI/UVN (narrow) and SBV fields of view represent staring-mode imager fields. The rectangles indicate projections of the FOVs onto a plane perpendicular to the line of sight and containing the center of the Earth. Even at low tangent altitudes, no field of view encompasses more than ~70 km in tangent altitude. The Earth limb presents an extreme intensity gradient, especially at low altitudes, and experiment planners must consider possible saturation in the lowest-altitude pixels as well as off-axis contamination. Unfortunately, interesting phenomena such as the aurora, polar mesospheric clouds, and gravity wave turbulence all occur at low-limb altitudes below ~150 km and must be observed against the limb intensity gradient.

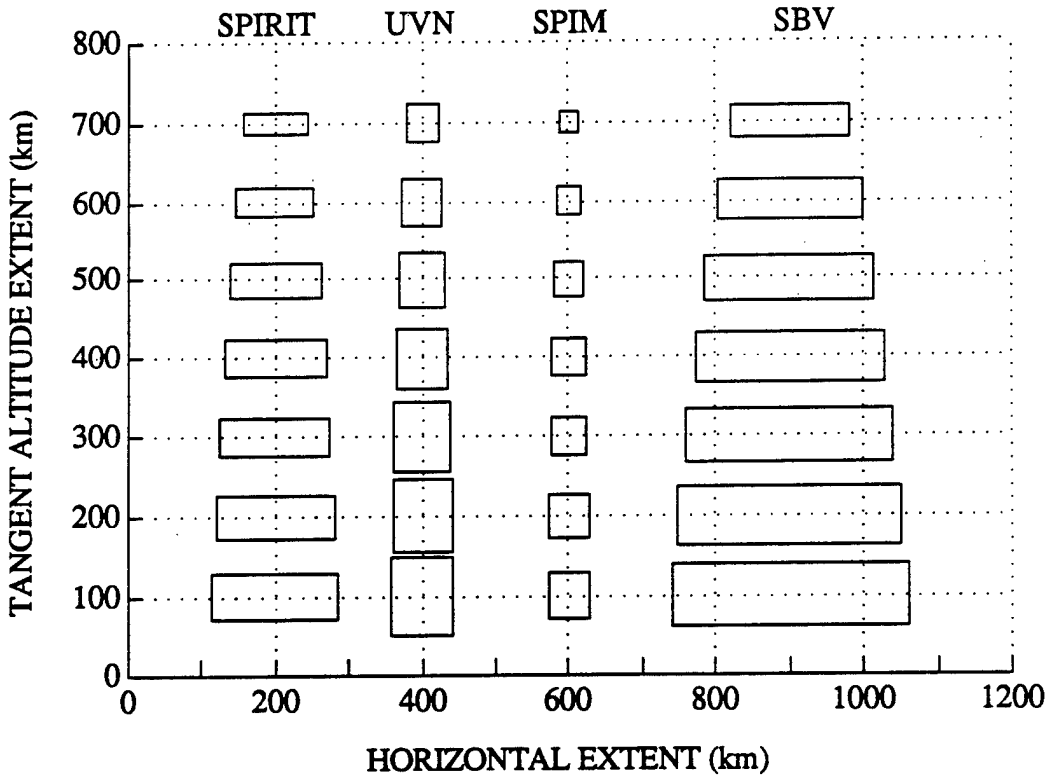

Fig.4-14. Comparison of fields of view of MSX instruments at various tangent altitudes.

To overcome limitations in the fields of view, the MSX platform will perform pitching or elevation maneuvers. These maneuvers will permit the instruments to make measurements through a useful range of altitudes. Figure 4-15 indicates several proposed limb scan patterns, which show how

the boresight of the satellite would change in tangent altitude. Four possible scan options are available. First, of course, the satellite could remain at a constant tangent altitude (here arbitrarily shown as ~210 km). In this pattern, the instruments would sample only a limited region of the atmosphere. This constant-elevation observation encorporates all "coolie-hat" scans required by the SPIRIT instrument. Second, a sawtooth scan would pitch the platform continuously up and down in tangent altitude. The Delta series of programs successfully employed this type of limb scan pattern to make limb observations. Third, a step-stare scan would "park" the fields of view at various altitudinal steps so the instruments could observe each altitude without the smearing effects possible in the sawtooth mode. Fourth, a track scan might would allow the instrument to follow a star (or target) through a continuous range of altitudes. The latter scan pattern could be used, for example, to observe the occultation of a star by the terrestrial atmosphere. Figure 3 shows sawtooth and step-stare scans moving through the full altitudinal range of the thermosphere (~100-500 km). However, to conserve spacecraft resources or re-scan altitudes, these scans could be limited to a smaller range in altitudes.

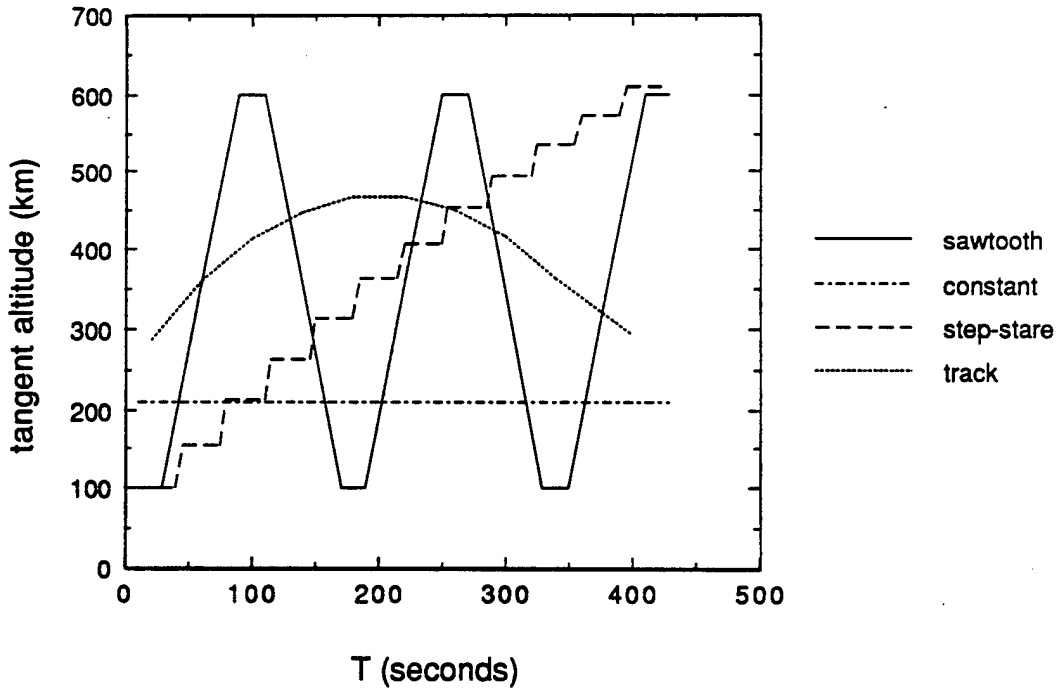

Fig.4-15. Several proposed limb scan patterns show the elevation angle change of the MSX platform.

During each of the scans, the orbital motion of the satellite itself would allow the instruments to sample in latitude. Therefore, the scan patterns would effectively produce a 2D mapping of the Earth limb emissions. Take altogether, these measurements would represent a comprehensive, long-term synoptic survey of the atmosphere. A video version of these measurements would indicate the "weather" of the upper atmosphere, much as time-lapse photographs show the development of weather in the lower atmosphere.

Table 4-3 summarizes the several types of limb-scans envisioned for Earth-limb measurements and suggests rates of motion. The ϕ angle refers to an azimuth angle in an orbit normal plane and measured counter-clockwise from the spacecraft velocity, while the θ angle is simply the zenith angle measured from the platform's Earth-radius vector. The ϕ_o angle is arbitrary. The subscripts indicate starting and stopping angles. In general, the lower limit of the elevation angle corresponds to a tangent altitude of ~100 km. (To conserve cryogen and ease pixel-saturation effects, the platform boresight should not regularly look below this altitude.) The angle rates must conform to spacecraft maneuvering limits and pixel-smearing constraints. Furthermore, all scan geometries must obey solar keep-out and ram restrictions. The table also includes a zenith observation mode for observing the airglow and geocorona above the spacecraft.

Table 4-3
EARTHLIMB SCANNING SUMMARY

Name	ϕ_1	ϕ_2	$d\phi/dt$	θ_1	θ_2	$d\theta/dt$
Coolie Hat Scan (CHS)	ϕ_o	ϕ_o+360°	TBD	<117°	θ_1	0
Coolie Hat Sector Scan (CHSS)	ϕ_o	ϕ_o+45°	TBD	<117°	θ_1	0
Coolie Hat Drift (CHD)	~90°	~90°	Orb*	<117°	θ_1	0
Coolie Hat Mirror Scan (CHMS)	ϕ_o	ϕ_o	Orb*	<117°	θ_1	0
Constant Zenith Angle (CZA)	ϕ_o	ϕ_o	Orb*	<117°	θ_1	0
Sawtooth (ST)	ϕ_o	ϕ_o	Orb*	117°	109°	<0.1°/s
Step-stare (SS)	ϕ_o	ϕ_o	Orb*	117°	109°	0
Track (T)	var	var	<Orb*	<117°	110°	var
Zenith (Z)	ϕ_o	ϕ_o	var	~0°	~0°	0

*Orb= orbital rate (=360°/101min= 0.059°/s)

4.3.4. EARTH LIMB SURVEY

The MSX program should conduct a long-term survey of the Earth limb backgrounds by regularly sampling selected tangent altitudes by orbital segment. That is, each observation would cover one orbital segment (see Fig. 4-11) and one type of limb scan (see Table 4-3). Each segment would occupy ~25 minutes of observational time, thus allowing the spacecraft to conserve power and thermal resources. Five segments a day on non-consecutive orbits would provide complete coverage of the northern hemisphere and part of the south. This observational scheme would consist of one polar segment, two mid-latitude segments (day and night), and two low-latitude segments (day and night), and would require 67.2 minutes of observing time (a daily duty cycle of 4.7%). However, given the importance of the polar regions to strategic defense, the Earthlimb observations should include longer and more frequent polar segments (~20 minutes two or three times a day). In the latter case, a the total Earthlimb budget would extend to 90.4 minutes (6.3% duty cycle).

Table 4-4 proposes three possible options for conducting an Earth-limb survey. Option 1 represents a minimal survey, while option 3 represents the optimal survey allowed by spacecraft resources (i.e., ~10% duty cycle with margin for non-survey observations). Option 2 is a compromise between the two.

Table 4-4
EARTHLIMB SURVEY OPTIONS

Segments	Option 1 (no. x min.)	Option 2 (no. x min.)	Option 3 (no. x min.)
Polar	1 x 16.8	2 x 20.0	3 x 20.0
Mid-Latitude	2 x 8.4	2 x 8.4	3 x 8.4
Low-Latitude	2 x 16.8	2 x 16.8	2 x 16.8
Total obs. time (min.)	67.2	90.4	118.8
Daily Duty Cycle	4.7 %	6.3 %	8.3 %

A full year of survey data would provide a complete four-season sampling of the middle and upper atmospheres. For example, polar mesospheric clouds could be observed during the summer after the solstice, while stratospheric warmings could be observed during the northern winters. Regular survey observations ensure the measurement of precursor and post-phenomena effects associated with PMCs and stratospheric warmings. The survey allows examination of effects caused by the seasonal "precession" of the geomagnetic dipole and auroral oval from predominantly sunlit

conditions to predominantly dark conditions. The revisiting of various tangent altitudes and sun-illuminations allows construction of a statistical model of Earthlimb radiances binned by latitude, longitude, and sun position. In addition, the regular measurement of limb PSDs will determine if the PSD depends of spectral bandpass, if it varies with latitude, and if

Two to four years of such contiguous coverage would extend the measurements over a significant portion of the solar cycle and would result in a comprehensive survey of the upper atmosphere. This survey would establish an extensive database from which investigators might build predictive or forecasting models.

4.3.5. EARTH LIMB ALERTS

Certain Earthlimb phenomena such as polar mesospheric clouds or stratospheric warmings occur either randomly or with seasonally dependent probability. For example, PMCs usually occur in the summer polar regions in the month following the solstice and may be most likely found on the western side of the polar cap, while stratospheric warmings occur in the winter months in the northern hemisphere. However, modern science cannot predict the occurrence, size, or exact location of a particular PMC or stratospheric warming.

The Space Environment Services Center (SESC) at the National Geophysical Data Center (Boulder, CO) provides notification that stratospheric warmings are underway but does not predict their occurrence nor their duration. These alerts originate from weather radar, balloon, and rocket measurements that occur regularly over Europe, the United States, and Canada. The SESC issues these notifications as part of its daily Solar and Geophysical Activity Summary, which is available on teletype or through computer networks.

By monitoring the SESC activity summaries, MSX investigators can ascertain when and approximately where a stratospheric warming is occurring. They can then command the spacecraft to enter a pre-approved observing sequence (possibly a coolie-hat sector scan centered on the warming event). Because the duration of the stratospheric warming is unknown, the spacecraft should execute this observing sequence as quickly as possible. The observation may pre-empt one of the regular survey observations, which can be re-scheduled on a successive orbit. If the stratospheric warming lasts long enough, MSX could observe its evolution through more than one orbit.

A similar centralized alert for polar mesospheric clouds does not exist, but ground-based observatories could alert the MSX mission the presence of noctilucent clouds observed overhead. MSX investigators should regularly contact remote observatories during the PMC season (e.g., College, AL, or Chatanika, Canada) to determine the location and status of any noctilucent clouds. Once the existence of the clouds has been ascertained, MSX could be commanded on its next orbit into a pre-approved PMC observational mode.

4.3.6. LOW LIMB AND NADIR

As discussed previously, "low limb" refers to that portion of the atmosphere below ~60 km that is not regularly observed during the cryogen portion of the mission. "Nadir" refers measurements at elevation angles below that of the Earth horizon at 0 km tangent altitude. Both low limb and nadir measurements should take place during the post-cryogen phase of the MSX mission and both would utilize the UVISI instrument.

Measurements of the low limb could easily be conducted during the regularly-scheduled limb scan observations merely by extending the elevation angle lower. Either the sawtooth or the step-stare pattern could be used. The low limb scans would permit the observation of the mesosphere, stratosphere, and troposphere. Low limb observations also ensure the measurement of the mesopause and the stratopause, both of which represent particularly important places for gravity wave and stratospheric and mesospheric clouds.

Nadir measurements fall into two categories. The first of these represents actual observation of the "hard Earth"; instruments operating at wavelengths longer ~300 nm can observe the surface of the Earth. The second category represents measurements of the terrestrial airglow and scattered sunlight; all the shortwave instruments can measure these atmospheric emissions. The nadir measurements will complement those of the limb. Together, these should provide an essentially 3D picture of the terrestrial atmosphere.

The MSX platform should conduct horizon-to-horizon scans at regular intervals during the post-cryogen phase. These scans should carry the fields of view from +100 km at one horizon, though nadir, to +100 km at the other horizon. This scanning would take place during one or more of the orbital segments. One such scan during a polar segment for example, would permit mapping of the complete auroral oval.

4.3.7. AURORA SURVEY

Auroral measurements fall into two principal categories. The first category consists of auroral observations conducted on a regular or survey basis during the normal polar segments. These observations represent scheduled measurements of the auroral backgrounds on which statistical studies of the auroral morphology rely. The second category consists of auroral observations conducted as the result of alerts issued by agencies such as the SESC. Auroral alert measurements will take place irregularly and will depend on placing the spacecraft in an observational mode on relatively short notice.

Regularly scheduled auroral observations take place during the polar segments of the MSX orbit and may be considered part of the normal Earth-limb survey. These observations could be included in the regular limb scan measurements or as separate measurements dedicated to auroral observations. If included as regular limb measurements during the polar segment, the aurora would be measured within the context of the normal

limb scanning patterns discussed in Section 4.3.3. However, the restriction of these scan patterns to 75-200 km altitudes would concentrate observations within the principal altitudes of auroral emissions and also allow measurement of polar mesospheric clouds.

During one of the daily polar segments, the UVISI image processor could acquire and track auroral features that might occur. To ensure maximum spatial coverage for acquiring auroral features, one of the UVISI WFOV imagers should be used. The UVISI IUW sensor should always be used for daytime auroral feature acquisition, while either the UVISI IUW or IVW imager would suffice for nighttime acquisition. Tracking auroral features across the polar terminator should employ the IUW imager. The WFOV imagers have special filters allowing the isolation of auroral features during daytime and nighttime conditions, and these filters would be employed during acquisition and tracking. The UVISI tracking, of course, will ensure that solar keep-out and tangent altitude restrictions are observed.

Regular observations permit the establishment of both spectrographic and morphological databases of the aurora. The spectrographic measurements will yield important information on the energy and fluxes of precipitating particles that cause the aurora, while the imaging measurements will provide information on the spatial extent and temporal evolution of the aurora. (UVISI offers the highest time resolutions of an space-based auroral imager.) The use of the UVISI image processor ensures that MSX instruments will observe discrete auroral features, so that dedicated auroral observations become quite important.

Spatial clutter from the aurora represents a central measurement of the MSX backgrounds experiments. Clutter observations will determine if the background radiance of the auroral PSD depends of spectral bandpass, if the PSD varies with location relative to the oval, how the PSD changes with auroral intensity, and if the auroral PSD differs from that observed at lower latitudes (i.e., does a universal PSD exist?).

4.3.8. AURORAL ALERT

The National Oceanic and Atmospheric Administration (NOAA) and the United States Air Force sponsor a number of programs that monitor and forecast conditions of the atmosphere, the ionosphere and the sun. The NOAA Space Environment Laboratory (SEL) and the USAF Air Weather Service (AWS) jointly issue prompt and standardized information on solar and geophysical phenomena that can be used by MSX investigators to determine the imminence of auroral activity.

The products of interest to MSX may be placed into two general categories: solar and geomagnetic. The solar category refers exclusively to conditions on the solar surface and within its corona. NOAA/SEL monitors solar activity through solar indices such as sunspot number or $F_{10.7}$ radio flux and through energetic particle and x-ray detectors on the GOES satellites. Any of these monitors of solar activity may serve as to predict geomagnetic conditions for aurora.

The geomagnetic category refers to variations in the magnetic field as observed by ground stations. NOAA/SEL issues provisional estimates of the planetary range indices A_p and K_p. These indices derive from real-time measurements of magnetometers at places such as College (Alaska), Goose Bay (Newfoundland), and Boulder (Colorado). However, these indices will differ from the "final" indices derived by the Institut für Geophysik in Göttingen, FRG, which uses a more extensive (and more representative) network of magnetometers. The predicted indices *do not* have a high level of reliability, however.

NOAA/SEL makes these solar and geomagnetic products available on time scales ranging from several hours to daily to weekly to monthly and provides real-time or near-real-time information for operational support. Products can be accessed by phone, computer network, modem, or by mail. The MSX users will generally supply any equipment necessary for the transfer of data, such as computer terminals, teletypes, modems, or radio receivers. Table 4-5 summarizes products of SEL's Space Environment Services Center.

Definitive prediction of auroral activity would require information from spacecraft located in interplanetary space well upstream of the earth's bow shock (>20 R_E from earth). The spacecraft would monitor the interplanetary magnetic field, solar wind pressure and temperature. and even then would only predict auroral activity in general as quantified by some auroral activity index such as AE, AU, or AL. Therefore, specific auroral activity, such as required for MSX experiments simply cannot be predicted. No pre-activity "tip-off" event exists.

Ground observations could indicate that an auroral or substorm event is in progress. Data from magnetic observatories, all-sky cameras (located throughout the northern hemisphere) or from radars (located at Chatnika and Goose Bay, Canada) could offer excellent indications of auroral activity occurring at their specific locations. To take advantage of these stations requires instantaneous communication the various observatories. Furthermore, the MSX satellite would have to overpass the station signalling the activity at the time the activity is occurring, which is possible but unlikely. MSX might attempt to communicate with a *limited* number of ground observatories (e.g., Goose Bay radar has a direct communication link to APL) at times when MSX passes within a few degrees of their observational fields of regard.

Space observations offer a better prospect for obtaining indications of auroral activity. The Defense Meteorological Satellite Program (DMSP) routinely makes slow-scan optical observations of the entire globe, from which one may deduce the near-realtime state of aurora (e.g., Akasofu, 1976). Furthermore, DMSS provides an "auroral oval alert" based on a statistical model and measurement of precipitating electrons (e.g., Hardy et al., 1985). The USAF Global Weather Center/Space Forecasting Center (Omaha) makes this information available to MSX through the space test range and could provide a direct, real-time teletype link. However, the DMSP observations represent relatively slow accumulations of data taken once per orbit (~100

Table 4-5a
AURORAL ALERT SUMMARY — 1

Item	Description	Schedule	Access
Preliminary Report & Forecast	Summary of activity and indices of prior week and forecast for next 27 days	weekly	US mail & teletype
Telephone Geoalert	Activity and indices for last 24 hours and next 24	updated every 3 hrs	Phone recording
Radio Alert	Activity and indices for last 24 hours and next 24	broadcast twice per hr	WWV radio
SESC Satellite	Activity and indices for last 24 hours and next 24	continuous broadcast	Satellite station
Real-time Alert Warning	Direct notification when various thresholds are met or exceeded	time of occurrence	telephone or teletype
Solar Coronal Disturbance Report	Information on possible coronal mass ejections and coronal holes	0200 UT every day	teletype
Satellite Anomaly Service	Assessment of space environment at time and place of satellite anomaly	as required by requestor	written report
Solar & Geophysical Activity Report & Forecast	Solar/geophysical activity and indices for last 24 hrs; predictions for next 72 hrs	2200 UT every day	teletype

minutes) and might not provide the quick response desired for MSX auroral observations.

The MSX imagers themselves could monitor auroral activity, either through the 1 Mbit downlink or through the regular limb scans. The operation of a UVISI WFOV imager during passes over the auroral regions would allow the instantaneous monitoring of auroral activity. During the nighttime, the UVISI WFOV visible imager would observe the aurora (probably using its 6300Å filter); during the day, the WFOV UV imager would observe the aurora (using the 1356-1493Å filter). The images would determine when and where to point MSX in order to make comprehensive auroral measurements. Possibly, MSX could be automated to respond to UVISI detections of aurora and operate independently of ground command.

Table 4-5b
AURORAL ALERT SUMMARY — 2

Item	Description	Schedule	Access
Solar Region Summary	Describes solar surface features of preceding day and predicts next 3 days	0030 UT every day	teletype
Solar & Geophysical Activity Summary	Particle events, indices, stratwarms, x-ray activity of preceding day	0245 UT every day	teletype
Geoalert	Encoded summaries and forecasts for international campaigns	0330 UT every day	teletype
Outlook	Predicted daily values of 27 day, 10 cm, A_p values	Every Tuesday	teletype
Data summaries	Encoded data and solar images (some customers)	Daily	US mail
Direct Inquiries	Contact duty forecaster	Anytime	telephone
SELDADS	SESC data acquisition & display system for solar and geomagnetic data	Anytime	computer network
Glossary of Terms	Definitions and standard usage terms	On request	US mail
Public Bulletin Board System	Solar/ionospheric forecasts and daily reports	Anytime	300/1200 Bd modem

Once auroral activity is detected or determined imminent, the MSX platform should enter an aurora acquisition mode. This mode should utilize the UVISI WFOV visible imager (557.7 nm filter) for nighttime acquisition and the UVISI WFOV ultraviolet imager (135.6 nm or Lyman-Birge-Hopfield band filter) for daytime acquisition. As MSX approaches the presumably active aurora oval, the UVISI image processor will take control of the platform and use the pertinent UVISI imager to acquire a suitable auroral enhancement. The WFOV imagers have sufficiently large fields of view that no platform scanning in elevation is required. The image processor will acquire and lock onto some particular auroral enhancement and follow it through its spatial and temporal evolution.

In the event that no feature is acquired during an alert, the MSX instruments may still make useful auroral measurements by observing the 100 km level near which optical auroral usually occur.

4.3.9. PRE-CRYOGEN PHASE MEASUREMENTS

The brief pre-cryogen phase of the mission permits at least the UVISI instruments with an opportunity to survey the lower atmosphere and its coupling with the middle and upper atmospheres. First, UVISI observations of gravity waves in the lower atmosphere can determine the PSD of such waves as a continuous function of altitude (from 0 km) and can suggest the dominant production mechanism of such waves so that they may be predicted and their effects on the upper atmosphere determined. Second, even a few nadir or near-nadir observations of the auroral oval will permit UVISI to sample the energy deposition rates over a spatially extended portion of the oval, to determine how auroral PSDs vary with energy dosing, and to establish benchmarks for locating the oval for future measurements during the cryogen phase. Third, the extension of UVISI scans below the 60 km altitude limit will allow a complete evaluation of its NRER function as well as its off-axis rejection curve.

Table 4-6 exhibits a number of possible observations for the pre-cryogen phase. Because these observations will occur soon after launch (possibly within a week), the launch date itself partially dictates which phenomena can be observed by UVISI and where. Essentially every launch date offers observational possibilities.

Table 4-6
POSSIBLE PRE-CRYOGEN OBSERVATIONS

Launch date	Observations	Place
January	Polar Mesospheric Clouds	Southern Polar Region
	Sunlit Auroral Oval	Southern Hemisphere
	Dark Auroral Oval	Northern Hemisphere
	Stratospheric Warmings	Northern Polar Region
	Break-up of Polar Vortex	Northern Polar Region
April	"Centered" Auroral Oval	Both Hemispheres
	Ozone Hole Breakup	Southern Hemisphere
July	Polar Mesospheric Clouds	Northern Polar Region
	Sunlit Auroral Oval	Northern Hemisphere
	Dark Auroral Oval	Southern Hemisphere
	Polar Vortex	Southern Hemisphere
October	Initial Stratospheric Warmings	Northern Polar Region
	"Centered" Auroral Oval	Both Hemispheres

4.3.10. SUMMARY OF EARTH LIMB MEASUREMENTS

Tables 4-7 through 4-10 summarize the measurements that SPIRIT, UVISI and SBV can undertake to provide a comprehensive survey of terrestrial background emissions. In each case, the tables indicate a specific measurement, specific observables, and the method utilized.

The short wavelength instruments can contribute in three ways to the measurement of terrestrial backgrounds. First, the spectrographic imagers can determine the compositional and thermodynamic state of the atmosphere by measuring both the major and minor species and their temperatures. Second, the imagers will determine the spatial extent and form of the auroral features. These observations will effectively determine the morphology of the aurora. Third, both the imagers and the spectrographic imagers will reveal the temporal evolution of the aurora. The 2-4 Hz sampling rates available will represent the fastest measurements of an aurora observed from space and will undoubtedly reveal important new processes.

In some instances, no more than a simple inversion of the spectral irradiance will recover the desired result, while other instances may require involved numerical, non-local thermodynamic equilibrium (non-LTE) calculations.

The tables indicate the relative importance of the spectrographic data to terrestrial background measurements. Because of this importance and since they represent a relatively small burden on spacecraft resources, the UVISI spectrographic imagers should be accorded a relatively high priority during any measurement of the backgrounds. Indeed, these instruments will also provide imaging information (albeit at a lower spatial and temporal resolution than the imagers) so that imagers should not completely dominate the observations of the terrestrial backgrounds.

Table 4-11 proposes a possible daily schedule for performing terrestrial background observations. The table assumes the MSX satellite will make 14 orbits per 24-hour period. Each entry in the table represents an observation of approximately one segment (Section 4.3.2). Italicized entries indicate observations made only during the post-cryogen phase; non-italic entries indicate the observations occur throughout the mission. Dashes denote periods of spacecraft allocated for recharging or periods relegated to other non-backgrounds observations. Note that the orbit segment approach allows full recharging to take place during the same orbit as the observation. Table headings indicate the types of observation. "Limb" refers to dedicated measurements of the limb backgrounds, while "aurora" refers to dedicated measurements of the aurora. The table reflects this increased capability by the addition of two extra auroral observations; the low limb observations represent extensions of the "quad" observations to lower altitudes and do not represent additional measurements.

Table 4-7

ATMOSPHERIC MEASUREMENTS FROM SPIRIT RADIOMETER

Measurement	Observation	Method
NO	NO(V)+O	IR spectral temperature
N_2O	$N_2(V)+O_2$, $N_2(A,V)+O_2$ (4.5, 6-10, 17-14 μm) N_2O+O (4.5, 6-10 μm)	IR spectrum and intensity IR spectrum and intensity IR time/intensity profile
N_2	N_2+e, N_2+O, N_2+N_2 (3-4 μm and 6-10 μm bands)	Infrared intensity and spectral distribution
OH	O_3+H, $O+H_2$, $O+HO_2$, $OH(V,J)+O$ (2.7, 10-24 μm)	Infrared intensity and spectral distribution
O_3	O_2+O_2, O_3+e (9.6 μm)	IR intensity
$T_{atmosphere}$	stratospheric warmings, aurora energization	IR spectral temperature

Table 4-8

ATMOSPHERIC MEASUREMENTS FROM SPIRIT INTERFEROMETER

Measurement	Observation	Method
CO	CO+N2(V), CO+O, CO+e CO(V)+O (4.3 μm) CO+N_2 (6-9 μm)	Infrared intensity and spectral distribution
CO_2	CO_2+O (15 μm)	IR intensity
OH	O_3+H, O+H_2, O+HO_2, OH(V,J)+O (2.7, 10-24 μm)	Infrared intensity and spectral distribution
H_2O	H_2O+e, H_2O+O, H_2O+hv (2.7 μm and17-24 μm bands)	Infrared intensity and spectral distribution
N_2	N_2+e, N_2+O, N_2+N_2 (3-4 μm and 6-10 μm bands)	Infrared intensity and spectral distribution
N_2O	N_2(V)+O_2, N_2(A,V)+O_2 (4.5, 6-10, 17-14 μm) N_2O+O (4.5, 6-10 μm)	IR spectrum and intensity IR spectrum and intensity IR time/intensity profile
NO	N(^{2}D)+O_2 (5.4, 2.7 μm)	IR spectral distribution
NO^+	N_2+O, O_2+NO,N(^{2}P)+O, N_2+O+O_2 (4.8 μm)	IR spectral distribution and intensity
O_3	O_2+O+M (9.6 μm) O_2+O_2, O_3+e (4.8, 9.6 μm)	IR spectral distribution

Table 4-9

ATMOSPHERIC MEASUREMENTS FROM UVISI SPECTROGRAPHIC IMAGERS

Measurement	Observation	Method
Neutral composition		
Daytime O	OI 130.4/164.1 nm	line ratio
	OI 130.4/135.6 nm	line ratio
	N_2 VK bands	quenching effects
Daytime N_2	N_2 LBH, 2PG bands	emission peak
Daytime O_2	N_2 LBH bands	O_2 SR absorption
Nighttime O	O_2 Herzberg I band	O+O reaction
Minor species		
Daytime NO	NO γ bands	Fluorescent scattering
Daytime N	NI 149.3, 174.3 nm	electron impact
Daytime Mg	MgI,II 285.2, 279.8 nm	resonant scattering
Day/night H	HI 121.6, 656.3 nm	resonant scattering
Nighttime N	NO δ bands	N+O
Nighttime NO	NO_2 continuum	N+O
Energy deposition		
Auroral electrons	N_2 2PG,LBH	electron impact
	N_2^+ 1NG	electron impact
Temperature		
Daytime	O_2 ATM	band profile
	OI 135.6 nm	scale height
	N_2 LBH, 2PG	scale height
Nighttime	OH Mienel	band profile
	O_2 ATM	band profile
Wave phenomena		
	OH (6,2) 825-860 nm	line ratio and spatial variations
	OH Meinel	
	O_2 ATM	
	OI 557.7 nm	

Table 4-10

ATMOSPHERIC MEASUREMENTS FROM UVISI AND SBV IMAGERS

Measurement	Observation	Method
Atmospheric waves		
Horizontal waves	IUN, IUW images	Spatial variation
Vertical waves	IUN, IUW images	Spatial variation
Spatial clutter		
UV high resolution	IUN images of limb	Fourier transformation
Vis high resolution	IVN, SBV limb images	Fourier transformation
UV low resolution	IUW images of limb	Fourier transformation
Vis low resolution	IVW images of limb	Fourier transformation
Noctilucent clouds		
Number	IUW,IVW images at	Count
Area	grazing incidence to	Geometric projection
Brightness	high latitude limb	Radiometry
Aurora		
Day morphology	IUW, IUN images	Total area and extent
Night morphology	IUW, IVW images	Total area and extent
Activity	IVW images (557.7nm)	IBC index (for example)
Detailed structure	IUN,IVN, SBV images	Time history

Table 4-11

PROPOSED SCHEDULE
EARTH BACKGROUND OBSERVATIONS

Orbit	Limb	Aurora	Other
1	Mid-lat (d)	-	-
2	-	N. polar	-
3	-	-	-
4	Mid-lat (n)	-	-
5	-	N. polar	-
6	-	-	*Low limb*
7	Mid-lat (d)	-	-
8	-	N. Polar	-
9	-	-	-
10	Equator (d)	-	-
11	-	Equator (n)	-
12	-	-	*Low limb*
13	-	-	-
14	-	-	-

4.4. IMPACT OF MSX MEASUREMENTS

4.4.1. IMPACT ON DATABASES

The MSX database will expand existing databases in two principal ways. First, the MSX data will dramatically increase the *quantity* of terrestrial backgrounds data available. Observing six times daily for a total of ~120 minutes each in their nominal modes, the spectrographic imagers alone will return over 1.24×10^{11} bytes over the course of the first full year of MSX operation; the imagers will return several thousand times as much if operated in a comparable manner. Second, the MSX data will increase the *quality* of terrestrial backgrounds data. In conducting its limb surveys, MSX instrumentation will provide unprecedented spatial, temporal, and spectral coverage. Although previous space missions have made measurements having higher spatial resolution, or higher temporal resolution, or higher spectral resolution, none have achieved simultaneously high spatial, temporal, and spectral resolution that MSX will.

The promulgation of MSX data to the community represents a task of the highest magnitude for data managers. The vast amounts of data represent a major encumbrance for even modern computing systems, and investigators will undoubtedly rely heavily on summary datasets that allow rapid data assimilation and survey.

4.4.2. IMPACT ON EMPIRICAL MODELS

The MSX measurements will impact terrestrial background models in three fundamental ways. First, the measurements will provide new inputs for empirical models such as MSIS, IRI, and even LOWTRAN, which needs validation at the short wavelengths. Second, the measurements will provide boundary conditions for first principles models such as TGCMs; these boundary conditions will place strong constraints that the models need for thorough validation. Third, MSX observations will promote the development of new models such as the strategic scene generation models (SSGMs), which have both empirical and theoretical aspects.

Short wavelength data from MSX will enable the revision of many empirical models including MSIS and IRI, which are de-facto community standards. In principal, inversion of the SW data can provide atmospheric temperature, composition, and ionization data required for an almost complete revision of these models. Current techniques have become sophisticated enough to enable the conversion of short wavelength radiances with a precision that rivals in situ measurements. Indeed, the optical measurement of atmospheric parameters may prove inherently more accurate than in situ measurements because of the known difficulties in gathering data with mass spectrometers and particle detectors.

Extended below the mesopause (~75 km) during the post-cryogen phase, MSX short wavelength observations can potentially extend the models through essentially all altitude regimes from the surface to the top of the thermosphere (~800 km). MSX measurements can thus validate attempts to

make low-altitude models (such as the USSA) continuous with high-altitude models (such as MSIS).

Furthermore, the MSX instruments offer the prospect of global or near-global measurements that will ameliorate the latitude and longitude restrictions suffered by current versions of empirical models. Because of the polar orbit of MSX, a program of regular background measurements ensures coverage at the critical high-latitude and polar regions where many empirical models still suffer from a deficiency of data.

MSX observations will also provide empirical models with a temporal resolution hitherto unavailable. The time scales of short wavelength measurements extend from one-half second through several months. The rapid observations of the imagers will undoubtedly have a major impact on dynamical models of aurora, simply because such fast images of the aurora have never been made from space before (and seldom made from the ground!). An extended mission of several years will allow MSX shortwave instruments to observe seasonal and solar-cyclic variations that may also impact the empirical models.

Finally, the MSX observations offer empirical models a totally new viewpoint: simultaneous measurement of spatial structure (images) *and* spectral structure (spectra). All empirical models produce essentially a two dimensional picture: composition vs. altitude, temperature vs. altitude, etc. These 2D pictures are statistically binned in latitude and longitude to produce a 3D model. However, the simultaneous measurement of spatial and spectral structure will produce an instantaneous 3D picture of the atmosphere. Empirical models of the aurora will especially benefit from this new observational capability.

4.4.3. IMPACT ON FIRST-PRINCIPLES MODELS

MSX short wavelength measurements will have both a direct impact and an indirect impact on first principles models.

The measurements will directly impact these theoretical models in two ways. First, the measurements will supply much-needed boundary conditions needed to initialize these models. In particular, TGCM and auroral intensity models need extensive and accurate boundary conditions for validation. Indeed, any first-principles model can be made to agree with observations by suitable contrivance of initial conditions; short wavelength measurements will provide known, restrictive initial conditions without any such contrivance. Second, comparison of the model's output with the observations will provide the essential validation of the model itself. Because of the three dimensional extent of the data, the so-called "3D" models will for the first time undergo an actual multi-dimensional validation. Furthermore, the time resolution available from SW data will, as in the case of the empirical models, provide a severe constraint on all dynamical models built from first principles.

The short wavelength measurements will indirectly impact first-principles models by influencing the empirical models they use. *All*

theoretical models rely on empirical models such as MSIS to provide temperature and composition information. These empirical models themselves will have undergone modification as a result of the short wavelength measurements. The improvement of the empirical models should improve the results of the first-principles models.

4.4.4. PROMOTION OF NEW MODELS

A new and exciting dataset such as that promised by MSX will promote the development of new models of the terrestrial atmosphere. These new models fall into two distinct categories: models now being built and requiring additional data, and models now being conceived and requiring the unique data of MSX.

Two examples of models currently being constructed are the Strategic Scene Generation Model (SSGM) and the Auroral Intensity Code (AURIC). The SSGM represents an ambitious effort to synthesize models of target signatures, natural backgrounds, and nuclear backgrounds into a single model (e.g., Heckathorn, 1989). This model will require extensive measurements of the airglow and aurora, both for input and for validation. AURIC represents an effort to model the intensities of auroral emissions given information on precipitating particles (e.g., Huffman, 1990). AURIC will benefit from the short wavelength measurements of auroral intensities as well as from their conversion to ionization and electron profiles. The spectrographic capabilities of UVISI are especially important for the development of such auroral intensity codes.

A new synoptic model of atmospheric emissions may result from the massive database available after several years' observations. This empirical model will differ from the other empirical models in that it will present the atmosphere exclusively in terms of its optical emissions, rather than in terms of composition or temperature. Because of the capabilities of the MSX instruments, this model will extend through a wide range of spatial, spectral, and temporal regimes. The model could place atmospheric emissions (as observed from space) on the same footing as atmospheric composition (as reflected in the MSIS model) or atmospheric temperature (as reflected in the USSA model). The synoptic model of atmospheric emissions would have a major impact not only on strategic defense systems, which would utilize the model directly to estimate natural backgrounds, but also on any observational system requiring know-ledge of such backgrounds.

4.4.5. SYNERGISM

The MSX measurements will promote a synergism between the longwave and shortwave regimes. Auroral observations clearly exemplify this synergism. The short wavelength observations of UVISI provide measurements of the energy input into the aurora, while the long wavelength observations of SPIRIT provide a measurement of the end result of this energy input in terms of atmospheric heating. In other words, UVISI measures system input and SPIRIT measures system output.

APPENDIX A4-1
SATELLITE OBSERVATIONAL DATABASES

Satellite observational databases relevent to MSX fall into two distinct categories: "service" databases and "science" databases. Service databases refer to databases deriving from satellites dedicated to providing a service such as weather monitoring, minerological surveying, or crop surveying. Science databases refer to databases deriving from satellites devoted primarily to scientific investigations. The distinction between these categories is not always clear, because service satellites can and have served scientific purposes.

Table A4-1 presents data available from service satellites. These data are held at NOAA archive facilities and represent a rich database for the investigation of atmospheric phenomena (e.g., Allison and Schnapf, 1983). Table A4-2 covers data available from various scientific satellites that made observations relevant to the MSX mission.

Table A4-1
SERVICE SATELLITE DATA
ON TERRESTRIAL BACKGROUNDS

Satellite	Launch Date	Instruments
Nimbus series	mid-1960's to 1970's	HIRS—high resolution infrared scanner SAMS— THIR— thermal high resolution IR radiometer ERB— Earth radiation budget LIMS— Limb infrared monitor of the stratosphere
TIROS & TIROS-N series	mid-1970's to present	AVHRR— advanced very hi-res radiometer SBUV— spectral backscattered ultraviolet ERBE— Earth radiation budget experiment SSU—
GOES series	1980's	VISSR—visible/infrared scanning radiometer VAS—
LANDSAT series	1970's to 1980's	MSS— multispectral scanner RBV— return beam vidicon TM— thematic mapper
DMSP series	1970's to present	OLS— optical line scanner
SPOT	1986	HRV— high resolution vidicon

Table A4-2

SCIENTIFIC SATELLITE DATA ON TERRESTRIAL BACKGROUNDS

Satellite	Launch Date	Instruments	Reference
OGO series	mid-1960's	FUV photometers	Chubb and Hicks (1970) 630 nm photometer
Apollo 16	1972	FUV spectrometer	Carruthers & Page (1976)
AE series	1972	2 channel photometers, NUV-NIR	Hays et al. (1973)
ISIS-2	1973	391 nm, 557.7 nm, 630 nm photometer	Cogger & Anger (1973)
STP78-1	1978	EUV spectrometer	Bowyer et al. (1981)
S3-4	1978	FUV spectrometer	Huffman et al. (1980)
KYOKKO	1978	FUV TV camera	Kaneda (1979)
SME	1981	MUV spectrometers	Thomas (1984)
DE-1	1981	FUV and visible	Frank et al. (1981) scan'd photometer
HILAT	1983	FUV and visible	Meng & Huffman (1984) x-track spectometers
POLAR BEAR	1986	FUV and visible	Meng & Huffman (1987) x-track spectrometers
Viking	1986	FUV photometric	Anger et al. (1987b) imager
Delta 180 181	1986	FUV-VIS spectrom UV-VIS st. imager	Carbary & Meng (1989) Carbary et al. (1989)

Optical instruments on various scientific satellites have steadily contributed to the database on background radiation. Simple photometers with narrowband filters made the earliest of these measurements. Exemplifying these, the photometers on the OGO satellites initially measured the Earth's airglow and aurora at selected wavelengths in the far ultraviolet and visible and permitted the spatial mapping of these emissions (Chubb and Hicks, 1970; Barth and Schaffner, 1970). Photometers on the AE series of satellites provided both wide-field (high sensitivity) and narrow-field (high spatial resolution) measurements of atmospheric emissions from 280 nm to 732 nm (Hays et al., 1973, 1988).

Satellite spectrometers have provided information on atomic and molecular species in the atmosphere. Among the earliest of these, the far ultraviolet spectrometer placed on the Moon by Apollo 16 surveyed the terrestrial backgrounds from ~50 nm to 150 nm and made the first ever measurements of airglow below 110 nm (Carruthers and Page, 1976). Much more sophisticated spectrometers became available at the end of the 1970's, with the launching of the Air Force satellites, S78-1 and S3-4. The spin-scanning spectrometer on S78-1 (Bowyer et al., 1981) measured the extreme ultraviolet dayglow from 35 nm to 140 nm and revealed significant latitudinal and temporal variations (e.g. Chakrabarti et al., 1983). The S78-1 instrument also made the first measurements of EUV emissions in the polar cap region (Chakrabarti, 1986). The S3-4 spectrometer, a twin Ebert-Fastie instrument, measured the terrestrial backgrounds at the slightly longer vacuum ultraviolet wavelengths (107-193 nm, 162-290 nm) at very good spectral resolution (~2 nm) (Huffman et al., 1980). The S3-4 instrument made seminal observations of the ultraviolet airglow and aurora, discovered evidence of ultraviolet spacecraft glow (Conway et al., 1987), and continues to prove a fruitful resource for auroral and aeronomic investigations (e.g., Ishimoto et al., 1989). The ultraviolet spectrometers (188-310 nm, 223-340 nm) on the Solar Mesosphere Explorer (SME) measured atmospheric emissions in the lower thermosphere and mesosphere and made the initial observations of ultraviolet light scattered from noctilucent clouds (Rusch et al., 1984; Thomas, 1984). More modern spectral measurements will utilize spectrographs such as those on the SDI Delta 181 satellite, which obtained a full limb spectrum in 0.2 s (Carbary and Meng, 1989).

Satellite imagers, especially the early ones, relied on platform spin to map out a two dimensional image in isolated wavebands. The ISIS-2 satellite made auroral and airglow measurements with spin-scanning photometers at 391.4 nm, 557.7 nm, and 630.0 nm (e.g., Cogger and Anger, 1973) and made the first observation of the entire auroral oval (Lui et al., 1975a). From much higher altitude, spin-scan photometers on the DE-1 satellite made spectacular images of the aurora, polar cap aurora, and geocorona at far ultraviolet wavelengths (e.g., Frank et al., 1981, 1982; Rairden et al., 1986; Frank and Craven, 1988). Similar photometers on the Swedish Viking satellite have made fairly fast observations aurora in the far ultraviolet and have actually observed the evolution of substorms in auroral emissions at these

wavelengths (Anger et al., 1987a,b; Murphree et al., 1987; Shepherd et al., 1990).

Satellite instruments also use cross-track scanning in conjunction with orbital motion to construct an image. Although inherently slow, this type of imaging can reveal suprisingly high spatial resolution. The broadband images from Air Force DMSP satellites have proven exceedingly useful for the analysis of auroral morphology (e.g., Akasofu, 1974, 1976; Holzworth and Meng, 1975; Meng and Lundin, 1986). The auroral scanning photometers on the HILAT and POLAR BEAR satellites extended auroral imagery from the nightside to the dayside by observing auroral emissions in the vacuum ultraviolet (Meng and Huffman, 1984, 1987). These latter instruments have movable gratings that permit the selection of various spectral bands, the appropriate selection of which permit, after deconvolution, the aeronomical measurement of atmospheric temperatures and densities (e.g., Strickland et al., 1989).

More recent satellites have used staring-mode imagers, which offer a much faster response. The ultraviolet television camera on the Japanese KYOKKO satellite made the first attempts at staring-mode auroral imagery, but did not return pictures of very high resolution (Kaneda, 1979). The recent Delta series of SDI satellites carried ultraviolet and visible imagers that provided staring-mode images of terrestrial airglow and Earth scenes in the ultraviolet and visible at frame rates up to 30 frames/s (e.g., Carbary et al., 1989).

APPENDIX A4-2
ACRONYMS FOR SECTION 4

AE	Atmospheric Explorer
AE	Auroral Electrojet index
AL	Auroral Electrojet index lower
AWS	Air Weather Service
AU	Auroral Electrojet index upper
AURIC	Auroral Intensity Code
BDC	Backgrounds Data Center
CDAW	Coordinated Data Analysis Workshop
CIRA	COSPAR International Reference Atmosphere
COESA	Committee on the extension of the Standard Atmosphere
COSPAR	Committee on Space Research
DE	Dynamics Explorer
DMSP	Defense Meteorological Satellite Program
DPC	Data Processing Center
ETS	Equinox Transition Study
EUV	Extreme Ultraviolet (10-100 nm)
FOV	Field of View
FUV	Far Ultraviolet (100-200 nm)
GOES	Geostationary Operational Environment Satellite
GSE	Ground Support Equipment
HITRAN	High resolution transmission model
IBC	International Brightness Classification
ICED	Ionospheric Conductivity and Electron Density
IGCM	Ionospheric General Circulation Model
ILF	Investigator Local Facility
IONCAP	Ionospheric Communications Analysis and Prediction
IRI	International Reference Ionosphere
JHU/APL	Johns Hopkins University Applied Physics Laboratory
K_p	K Planetary index
LBH	Lyman-Birge-Hopfield
LOWTRAN	Low resolution transmission model
LTE	Local Thermodynamic Equilibrium
LWIR	Long Wavelength Infrared
MCC	Mission Control Center
MET	Mission Event Time
MLT	Magnetic Local Time
MPC	Mission Processing Center
MSIS	Mass Spectrometer and Incoherent Scatter
MSX	Midcourse Space Experiment
MUV	Middle Ultraviolet (200-300 nm)
NCAR	National Center for Atmospheric Research
NFOV	Narrow Field of View

NLC	Noctilucent Clouds
NOAA	National Oceans and Atmospheres Administration
NRL	Naval Research Laboratory
NSSDC	National Space Science Data Center
NUV	Near Ultraviolet (300-400 nm)
OGO	Orbiting Geophysical Observatory
PMC	Polar Mesospheric Clouds
QLF	Quick-look Facility
SBV	Space-based Visible
SEL	Space Environment Laboratory
SME	Solar Mesospheric Explorer
SMRD	Science Modeling Requirements Document
SPIM	Spectrographic Imager
SSGM	Strategic Scene Generation Model
STB	Short Wavelength Terrestrial Backgrounds
SR	Schumann-Runge
SW	Short Wavelength (<1000 nm)
TEC	Total Electron Content
TFM	Transfer Function Model
TGCM	Thermospheric General Circulation Model
UCL	University College London
USSA	United States Standard Atmosphere
UT	Universal Time
UVISI	Ultraviolet and Visible Imaging and Spectrographic Imaging
UVN	Ultraviolet Narrow Field of View
UVW	Ultraviolet Wide Field of View
VK	Vegard-Kaplan
WFOV	Wide Field of View

REFERENCES FOR SECTION 4

Akasofu, S.-I., The development of the auroral substorm, *Planet. Space Sci., 12*, 273-282, 1964.

Akasofu, S.-I., Dynamic morphology of the auroral substorm, *Space Sci. Rev., 4*, 498-540, 1965.

Akasofu, S.-I., *Polar and Magnetospheric Substorms*, D. Reidel, Dordrecht-Holland, 1968.

Akasofu, S.-I., A study of auroral displays photographed from the DMSP-2 satellite and from the Alaska meridian chain of stations, *Space Sci. Rev., 16*, 617-725, 1974.

Akasofu, S.-I., Recent progress in studies of DMSP auroral photographs, *Space Sci. Rev., 19*, 169-215, 1976.

Alder-Golden, S.M., M.W. Matthew, D.R. Smith, A.J. Ratkowski, The 9- to 12-μm atmospheric ozone emission observed in the SPIRIT I experiment, *J. Geophys. Res., 95*, 15243-15250, 1990.

Allison, L.J., and A. Schnapf, Meterological Satellites, in *Manual of Remote Sensing, Vol. 1*, ed. R. N. Colwell, American Society of Photogrammetry, pp. 651-679, 1983.

Anderson, D.E., Jr., and D.J. Strickland, Synthetic dayglow spectra and the Rayleigh scattering background from the far UV to the visible, *Ultraviolet Technology III*, R.E. Huffman, ed., Proc. SPIE 932, 170-176, 1988.

Anger, C. D., J.S. Murphree, A. Vallance-Jones, R.A. King, A.L. Broadfoot, L.L. Cogger, F. Creutzberg, R.L. Gattinger, G. Gusstafsson, F.R. Harris, J.W. Haslett, E.J. Llewellyn, J.C. McConnel, D.J. McEwen, E.H. Richardson, G. Rostoker, B.R. Sandel, G.G. Shephard, D. Venkatesan, D.D. Wallis, G. Witt, Scientific results from the Viking ultraviolet imager: an introduction, *Geophys. Res. Lett., 14*, 383-386, 1987a.

Anger, C.D., S.K. Babey, A.L. Broadfoot, R.G. Brown, L.L. Cogger, R. Gattingger, J.W. Haslett, R.A. King, D.J. McEwen, J.S. Murphree, E.H. Richardson, B.R. Sandel, K. Smith, A. Valance Jones, An ultraviolet auroral imager for the Viking spacecraft, *Geophys. Res. Lett., 14*, 387-390, 1987b.

Balsley, B.B., and D.A. Carter, The spectrum of atmospheric velocity fluctuations at 8 km and 86 km, *Geophys. Res., Lett., 9*, 465-468, 1982.

Barth, C.A., Rocket measurements of the nitric oxide dayglow, *J. Geophys. Res., 69*, 3301-3303, 1964.

Barth, C.A., and S. Schaffner, OGO4 spectrometer measurements of the tropical ultraviolet airglow, *J. Geophys. Res., 75*, 4299-xxxx, 1970.

Bates, D.R., Excitation of the 557.7 nm OI line in nightglow, *Planet. Space Sci., 36*, 883-889, 1988.

Bowyer, S., R. Kimble, F. Paresce, M. Lampton, G. Penegor, Continuous-read-out extreme-ultraviolet airglow spectrometer, *Appl. Opt., 20*, 477-xxx, 1981.

Butchart, N., S.A. Clough, T.N. Palmer, P.J. Trevelyan, Simulations of an observed stratospheric warming with quasi-geostrophic refractive index as a model diagnostic, *Quart. J. Roy. Met. Soc., 108*, 475-502, 1982.

Carbary, J.F., and C.-I. Meng, Limb profiles from low Earth orbit, *Ultraviolet Technology III*, R.E. Huffman, ed., Proc. SPIE 1158, 51-58, 1989.

Carbary, J.F., G.H. Fountain, J.S. Hansen, D.E. Fort, C.-I. Meng, Ultraviolet and visible wavelength measurements from low Earth orbit, *APL Tech. Dig., 10*, 56-65, 1989.

Carruthers, G.R., and T. Page, Apollo 16 far ultraviolet spectra of the terrestrial airglow, *J. Geophys. Res., 81*, 1683-xxxx, 1976.

Chakrabarti, S., F. Paresce, S. Bowyer, R. Kimble, S. Kumar, The extreme ultraviolet dat airglow, *J. Geophys. Res., 88*, 4898-xxxx, 1983.

Chakrabarti, S., Extreme and far ultraviolet emissions from the polar cap, *J. Geophys. Res., 91*, 8065-xxxx, 1986.

Chamberlain, J.W., *Physics of the Aurora and Airglow*, Academic Press, New York, 1961.

Chamberlain, J.W., *Theory of Planetary Atmospheres, An Introduction to their Physics and Chemistry*, Academic Press, New York, 1978.

Chanin, M.-L., and A. Hauchecarne, Lidar observation of gravity and tidal waves in the stratosphere and mesosphere, *J. Geophys. Res., 86*, 9715-9721, 1981.

Charney, J.G., and P.G. Drazin, Propagation of planetary-scale disturbances from the lower into the upper atmosphere, *J. Geophys. Res., 66,* 83-109, 1961.

Chubb, T.A., and G.T. Hicks, Observations of the aurora in the far ultraviolet from OGO 4, *J. Geophys. Res., 75,* 1290-xxxx, 1970.

Clough, S.A., F.X. Kneizys, E.P. Shettle, G.P. Anderson, Atmospheric radiance and transmittance: FASCOD2, in *Sixth Conference on Atmospheric Radiation, May 13-16, 1986,* American Meteorological Society, Boston, MA, 1987.

Clough, S.A., F.X. Kneizys, G.P. Anderson, E.P. Shettle, J.H. Chetwynd, L.A. Hall, FASCOD3: spectral simulation, in *IRS '88: Current Problems in Atmospheric Radiation,* ed. J. Lenoble and J.F. Geleyn, Deepak Publishing, Hampton, VA, 372-375, 1989.

Cogger, L.L., and C.D. Anger, The OI 5577Å airglow experiment on the ISIS-2 satellite, *J. Atmosph. Terr. Phys., 35,* 2081-xxxx, 1973.

Conway, R.R., R.R. Meier, D.F. Strobel, R.E. Huffman, The far ultraviolet vehicle glow of the S3-4 satellite, *Geophys. Res. Lett., 14,* 628-631, 1987.

Conway, R.R., and A.B. Christensen, The ultraviolet dayglow at solar maximum, 2, Photometer observations of N_2 second positive (0,0) band emission, *J. Geophys. Res., 90,* 6601-6607, 1985.

Committee on Extension of the Standard Atmosphere (COESA), *U.S. Standard Atmosphere, 1962,* U.S. Government Printing Office, Washington, DC, 1962.

Committee on Extension of the Standard Atmosphere (COESA), *U.S. Standard Atmosphere Supplements, 1966,* U.S. Government Printing Office, Washington, DC, 1966.

Committee on Extension of the Standard Atmosphere (COESA), *U.S. Standard Atmosphere, 1976,* U.S. Government Printing Office, Washington, DC, 1976.

COSPAR Working Group IV, *COSPAR International Reference Atmosphere, 1961 (CIRA 1961),* North Holland Publishing Co., Amsterdam, 1961.

COSPAR Working Group IV, *COSPAR International Reference Atmosphere, 1965 (CIRA 1965),* North Holland Publishing Co., Amsterdam, 1965.

COSPAR Working Group IV, *COSPAR International Reference Atmosphere, 1972 (CIRA 1972)*, North Holland Publishing Co., Amsterdam, 1972.

COSPAR Working Group IV, *COSPAR International Reference Atmosphere, 1986 (CIRA 1986)*, North Holland Publishing Co., Amsterdam, 1986.

Coulson, K.L., Characteristics of the radiation emerging from the top of the atmosphere- I. Intensity and polarization, *Planet. Space Sci., 1*, 265-276, 1959a.

Coulson, K.L., Characteristics of the radiation emerging from the top of the atmosphere- II. Total upward flux and albedo, *Planet. Space Sci., 1*, 277-xxx, 1959b.

Cunnold, D.M., F. Alyea, R.G. Prinn, A three-dimensional dynamical chemical model of atmospheric ozone, *J. Atmos. Sci., 32*, 170-194, 1975.

Degges, T.C., and H.J.P. Smith, A High-Altitude Infrared Radiance Model (HAIRM), Air Force Geophysics Laboratory, Hanscom Air Force Base, MA, AFGL-TR-77-0271, 1977.

Dickinson, R.E., E.C. Ridley, R.G. Roble, A three-dimensional, time-dependent general circulation model of the thermosphere, *J. Geophys. Res., 86*, 1499-1512, 1981.

Dickinson, R.E., E.C. Ridley, R.G. Roble, Thermospheric general circulation with coupled dynamics and composition, *J. Atmos. Sci., 41*, 205-219, 1984.

Dunkerton, T.J., C.-P.F. Hsu, M.E. McIntyre, Some Eulerian and Lagrangian diagnostics for a model stratospheric warming, *J. Atmos. Sci., 38*, 819-843, 1981.

Eather, R.H., and S.-I. Akasofu, Characteristics of polar cap auroras, *J. Geophys. Res., 74*, 4794-4798, 1969.

Feldstein, Y.I., Some problems concerning the morphology of auroras and magnetic disturbances at high latitudes, *Geomag. Aeron., 3*, 183-192, 1963 (in English).

Feldstein, Y.I., Peculiarities in the auroral distribution in high latitudes caused by the asymmetrical form of the magnetosphere, *Planet. Space Sci., 14*, 121-130, 1966.

Feldstein, Y.I., and N.F. Shevnina, Some results of visual observations of auroras in the northern hemisphere during the IGY-IGC period, *Geomag. Aeron.*, 3, 547-556, 1963 (in English).

Feldstein, Y.I., and G.V. Starkov, Dynamics of auroral belt and polar geomagnetic disturbances, *Planet. Space Sci.*, *15*, 209-229, 1967.

Feldstein, Y.I., and Yu. I. Galperin, The auroral luminosity structure in the high-latitude upper atmosphere: Its dynamics and relationship to the large-scale structure of the Earth's magnetosphere, *Rev. Geophys.*, 23, 217-275, 1985.

Fesen, C.S., R.E. Dickinson, R.G. Roble, Simulation of thermospheric tides at equinox with the NCAR thermospheric general circulation model, *J. Geophys. Res.*, *91*, 4471-4489, 1986.

Fogle, B., and B. Haurwitz, Noctilucent clouds, *Space Sci. Rev.*, *6*, 279-340, 1966.

Forbes, J.M., R.G. Roble, F.A. Marcos, Thermospheric dynamics during the March 22, 1979, magnetic storm, 2. Comparisons of model predictions with observations, *J. Geophys. Res.*, *92*, 6069-6081, 1987.

Frank, L.A., J.D. Craven, K.L. Ackerson, M.R. English, R.H. Eather, R.L. Carovillano, Global auroral imaging instrumentation for the Dynamics Explorer mission, *Space Sci. Instr.*, 5, 369-xxx, 1981.

Frank., L.A., J.D. Craven, J.L. Burch, J.D. Winningham, Polar views of the Earth's aurora with Dynamics Explorer, *Geophys. Res. Lett.*, *9*, 1001-1004, 1982.

Frank, L.A., and J.D. Craven, Imaging results from Dynamics Explorer 1, *Rev. Geophys.*, *26*, 249-283, 1988.

Fritts, D.C., Gravity wave saturation in the middle atmosphere: a review of theory and observations, *Rev., Geophys. Space Phys.*, 22, 275-308, 1984.

Fuller-Rowell, T.J., and D. Rees, A three-dimensional, time-dependent global model of the thermosphere, *J. Atmos. Sci.*, 37, 2545-2657, 1980.

Fuller-Rowell, T.J., and D. Rees, A three-dimensional, time-dependent simulation of the global dynamical response of the thermosphere to a geomagnetic substorm, *J. Atmos. Terr. Phys.*, 43, 701-721, 1981.

Fuller-Rowell, T.J., and D. Rees, Derivation of a conservation equation for mean molecular weight for a two-contituent gas within a three-dimensional, time-dependent model of the thermosphere, *Planet. Space Sci., 31,* 1209-1222, 1983.

Fuller-Rowell, T.J., D. Rees, S. Quegon, R.J. Moffett, G.J. Bailey, Interactions between neutral thermospheric composition and the polar ionosphere using a coupled ionosphere-thermosphere model, *J. Geophys. Res., 92,* 7744-7748, 1987.

Gadsen, M., Noctilucent clouds, *Space Sci. Rev., 33,* 279-334, 1982.

Gage, K.S., and T.E. Van Zandt, Wind measurement techniques available for the middle atmosphere program, *J. Geophys. Res., 86,* 9591-9598, 1981.

Garcia, R.R., Dynamics, radiation, and photochemistry in the mesosphere: implications for the formation of noctilucent clouds, *J. Geophys. Res., 94,* 14605-14615, 1989.

Geller, M.A., Modeling the middle atmosphere circulation, in *Dynamics of the Middle Atmosphere,* ed. J.R. Holton and T. Matuno, Terra Scientific Publications, Tokyo, 467-500, 1984.

Gussenhoven, M.S., D.A. Hardy, H. Heinemann, Systematics of the equatorward diffuse auroral boundary, *J. Geophys. Res., 88,* 5692-xxxx, 1983.

Hansen, J.E., and L.D. Travis, Light scattering in planetary atmospheres, *Space, Sci. Rev., 16,* 527-xxx, 1974.

Harris, I., and W. Priester, Theoretical models for the folar-cycle variation of the upper atmosphere, *J. Geophys. Res., 67,* 4585-4591, 1962a.

Harris, I., and W. Priester, Time-dependent structure of the upper atmosphere, *J. Atmos. Sci., 19,* 286-xxx, 1962b.

Hardy, D.A., M.S. Gussenhoven, E. Holeman, A statistical model of auroral electron precipitation, *J. Geophys. Res., 90,* 4229-xxxx, 1985.

Hays, P.B., G. Carignan, B.C. Kennedy, G.G. Shepherd, J.C.G. Walker, The visible airglow experiment on Atmospheric Explorer, *Radio Sci.,8,* 369-xxx, 1973.

Hays, P.B., V.J. Abreu, S.C. Solomon, J.-H. Yee, The visible airglow experiment- a review, *Planet. Space Sci., 36,* 21-35, 1988.

Heckathorn, H., The strategic scene generation model, presented at IRIS conference, Naval Post-graduate School, Monterey, CA, February 1989.

Hedin, A.E., A revised thermospheric model based on mass spectrometer and incoherent scatter data: MSIS-83, *J. Geophys. Res., 88,* 10170-10188, 1983.

Hedin, A.E., MSIS-86 thermospheric model, *J. Geophys. Res., 92,* 4649-4662, 1987.

Hedin, A.E., Atomic oxygen modelling in the upper thermosphere, *Planet. Space Sci., 36,* 907-920, 1988.

Hedin, A.E., H.G. Mayer, C.A. Reber, G.R. Carignan, N.W. Spencer, A global empirical model of thermospheric composition based on OGO-6 mass spectrometer measurements, *Space Res., 13,* 315-320, 1973.

Hedin, A.E., H.G. Mayer, C.A. Reber, N.W. Spencer, Empirical model of global thermospheric temperatire and composition based on data from the OGO-6 quadrapole mass spectrometer, *J. Geophys. Res., 79,* 215-225, 1974.

Hedin, A.E., J.E. Saleh, J.V. Evans, C.A. Reber, G.P. Newton, N.W. Spencer, D.C. Kayser, D. Alcayde, P. Bauer, L. Cogger, J.P. McClure, A global thermospheriuc model based on mass spectrometer data and ioncoherent scatter data, MSIS 1, N_2 density and temperature, *J. Geophys. Res., 82,* 2148-2156, 1977a.

Hedin, A.E., C.A. Reber, G.P. Newton, N.W. Spencer, H.C. Brinton, H.G. Mayr, W.E. Potter, A global thermospheriuc model based on mass spectrometer data and ioncoherent scatter data, MSIS 2, Composition, *J. Geophys. Res., 82,* 2148-2156, 1977b.

Hedin, A.E., C.A. Reber, N.W. Spencer, H.C. Brinton, D.C. Kayser, Global model of longitude/UT variations in thermospheric composition and temperature based on mass spectrometer data, *J. Geophys. Res., 84,* 1-9, 1979.

Hedin, A.E., and G. Thuillier, Comparison of OGO-6 measured thermospheric temperatures with the MSIS-86 empirical model, *J. Geophys. Res., 93,* 5965-5971, 1988.

Hines, C.O., *The Upper Atmosphere in Motion,* American Geophysical Union, Washington, DC, 1974.

Holton, J.R., *An Introduction to Dynamic Meteorology,* Academic Press, New York, 1972.

Holton, J.R., A semi-empirical model for wave-driven field flow interactions in the stratosphere: application to sudden stratospheric warmings, *J. Atmos. Sci., 33*, 1639-1649, 1976.

Holton, J.R., and W.M. Wehrbein, A numerical model of the zonal mean circulation of the middle atmosphere, *Pure Appl. Geophys., 118*, 284-306, 1980.

Holzworth, R.H., and C.-I. Meng, Mathematical representation of the auroral oval, *Geophys. Res. Lett., 2*, 377-380, 1975.

Holzworth, R.H., Auroral boundary variations and the interplanetary magnetic field, *Planet. Space Sci., 32*, 25-xx, 1984.

Hooke, W.H., Rossby-planetary waves, tides, and gravity waves in the upper atmosphere, in *The Upper Atmosphere and Magnetosphere*, Geophysics Reseach Board, National Academy of Sciences, Washington, DC, 1977.

Huffman, R.E., AURIC, presented at Short Wavelength Phenomenology Conference, Johns Hopkins University Applied Physics Laboratory, June 1990.

Huffman, R.E., F.J. LeBlanc, J.C. Larrabee, D.E. Paulson, Satellite vacuum ultraviolet airglow and auroral observations, *J. Geophys. Res., 85*, 2201-2215, 1980.

Hugenin, R., M. Wohlers, M. Weinberg, R. Huffman, R. Eastes, F. Delgreco, Spatial characteristics of airglow and solar scatter radiance from the Earth's atmosphere, in *Ultraviolet Technology III*, ed. R.E. Huffman, proc. SPIE 1158, 16-27, 1989.

Ishimoto, M., C.-I. Meng, G.R. Romick, R.E. Huffman, Doppler shift of auroral Lyman α observed from a satellite, *Geophys. Res. Lett., 16*, 143-146, 1989.

Jacchia, L.G., A variable atmosphere-density model from satellite accelerations, *J. Geophys. Res., 65*, 2775-2782, 1960.

Jacchia, L.G., Static diffusion models of the upper atmosphere with empirical temperatire profiles, *Smithsonian Contr. Astrophys., 8*, 215-xxx, 1965.

Jacchia, L.G., New static models of the thermosphere and exosphere with empirical temperature profiles, Special Report 313, Smithsonian Astrophys. Obs., Cambridge, MA, 1970.

Jacchia, L.G., Revised static models of the thermosphere and exosphere with empirical temperature profiles, Special Report 332, Smithsonian Astrophys. Obs., Cambirdge, MA, 1971.

Jacchia, L.G., Thermospheric temperature, density, and composition: new models, Special Report 375, Smithsonian Astrophys. Obs., Cambridge, MA, 1972.

Jaccia, L.G., Thermospheric temperature, density, and composition: new models, Special Report 375, Smithsonian Astrophys. Obs., Cambridge, MA, 1977.

Jacchia, L.G., J.W. Slowlet, U. von Zahn, Thermospheric seasonal-latitudinal variations of four major atmospheric constituents from ESRO 4 gas analyzer measurements, *Space Res. XVIII*, 199-206, 1978.

Jensen, E., G.E. Thomas, O.B. Toon, On the diurnal variation of noctilucent clouds, *J. Geophys. Res., 94*, 14693-14702, 1989.

Kamide, Y., Relationship between substorms and storms, in *Dynamics of the Magnetosphere*, S.-I. Akasofu, ed., D. Reidel, Dordrecht-Holland, pp. 425-443, 1980.

Kamide, Y., and J.D. Winningham, A statistical study of the "instantaneous" nightside auroral oval: The equatorward boundary of electron precipitation as observed by the ISIS 1 and ISIS 2 satellites, *J. Geophys. Res., 82*, 5573-5588, 1977.

Kneizys, F.X., E.P. Shettle, L.W. Abreu, J.H. Chetwynd, G.P. Anderson, W.O. Gallery, J.E.A. Selby, S.A. Clough, User's Guide to LOWTRAN7, Air Force Geophysics Laboratory, AFGL-88-0177, ADA206773, 1988.

Kaneda, E., Auroral TV observations by KYOTTO, Proc. of Internat'l. Workshop on Selected Topics of Magnetospheric Physics, Japanese IMS Committee, p. 15, 1979.

Killeen, T.L., Energetics and dynamics of the Earth's thermosphere, *Rev. Geophys., 25*, 433-454, 1987.

Kroehl, H.W., and B.A. Hausman, An Ionospheric Conductivity and Electron Density Profile Model - Phase II, System Documentation Users' Manual, Solar-terrestrial Physics Division, National Geophysical Data Center, Boulder, CO, 1986.

Labitzke, K., Climatology of the stratosphere and mesosphere, *Phil. Trans. Roy. Soc. London A, 296*, 7-18, 1980.

Labitzke, K., Stratospheric-mesospheric mid-winter disturbances: a summary of observed characteristics, *J. Geophys. Res., 86,* 9665-9678, 1981.

Lindzen, R.S., Turbulence and stress owing to gravity wave and tidal breakdown, *J. Geophys. Res., 86,* 9707-9714, 1981.

Lindzen, R.S., and D. Blake, Mean heating of the thermosphere by tides, *J. Geophys. Res., 75,* 6868-xxxx, 1970.

Lui, A.T.Y., C.D. Anger, D. Venkatesan, W. Sawchuk, S.-I. Akasofu, The topology of the auroral oval as seen by the ISIS 2 scanning auroral photometer, *J. Geophys. Res., 80,* 1795-xxxx, 1975a.

Lui, A.T.Y., C.D. Anger, S.-I. Akasofu, The equatorward boundary of the diffuse aurora and auroral substorms as seen by the ISIS 2 auroral scanning photometer, *J. Geophys. Res., 80,* 3602-xxxx, 1975b.

Malkmus, W., J.P. Filice, C.B. Ludwig, Earthlimb radiances, transmissivities, and clutter, in *Ultravciolet Technology III,* ed. R.E. Huffman, Proc. SPIE 1158, 69-83, 1989.

Manson, A.H., C.E. Meek, and J.B. Gregory, Winds and waves (10 min- 30 days) in the mesosphere and lower thermosphere at Saskatoon (52°N, 107° W, L=4.3) during the year, October 1979 to July 1980, *J. Geophys. Res., 86,* 9615-9625, 1981.

Matsuno, T., A dynamical model of the stratospheric sudden warming, *J. Atmos. Sci., 28,* 1479-1494, 1971.

Mayr, H.G., I. Harris, F. Varosi, F. A. Herrero, Global excitation of wave phenomena in a dissipative multicomponent medium, 1. Transfer function of the Earth's thermosphere, *J. Geophys. Res., 89,* 10929-10959, 1984.

Mayr, H.G., I. Harris, F. Varosi, F.A. Herrero, Global excitation of wave phenomena in a dissipative multicomponent medium, 2. Impulsive perturbations in the Earth's thermosphere, *J. Geophys. Res., 89,* 10967-10986, 1984.

Meier, R.R., R.R. Conway, D.E. Anderson, Jr., P.D. Feldman, R.W. Eastes, E.P. Gentieu, A.B. Christensen, The ultraviolet dayglow at solar maximum, 3, photoelectron-excited emissions of N_2 and O, *J. Geophys. Res., 90,* 6608-6616, 1985.

Meng, C.-I., and R.E. Huffman, Ultraviolet imaging from space of the aurora under full sunlight, *Geophys. Res. Lett., 11*, 315-318, 1984.

Meng, C.-I., and R. Lundin, Auroral morphology of the midday oval, *J. Geophys. Res., 91*, 1572-xxxx, 1986.

Meng, C.-I., and R.E. Huffman, Preliminary observations from the auroral and ionospheric remote sensing imager, *APL Tech. Dig., 8*, 303-307, 1987.

Murphree, J.S., L.L Cogger, C.D. Anger, D.D. Wallis, G.G. Shepherd, Oval intensifications associated with polar arcs, *Geophys. Res. Lett., 14*, 403-406, 1987.

Nadile, R.M., and A. J. Ratkowski, Observations of auroral spectral structure, in *Proceedings of the Tri-Services Infrared Backgrounds Symposium*, ed. R.M. Murphy and T.D. Conley, AFGL-TR-84-0094, March 1984.

Nakai, H., Y. Kamide, D.A. Hardy, M.S. Gussenhoven, Time scales of expansion and contraction of the auroral oval, *J. Geophys. Res., 91*, 4437-4450, 1986.

Olivero, J.J., J.J. Tsoum C.L. Croskkey, L.C. Hale, R.G. Joiner, Solar absorption microwave measurement of upper atmosphere water vapor, *Geophys. Res., Lett., 13*, 197-200, 1986.

Palmer, T.N., Aspects of stratospheric sudden warmings studied from a transformed Eulerian-mean viewpoint, *J. Geophys. Res., 86*, 9679-9687, 1981.

Pemberton, E.V., and G.G. Shepherd, Spatial characterisitcs of auroral brightness fluctuation spectra, *Can. J. Phys., 53*, 504-513, 1975.

Philbrick, C.R., K.U. Grossman, R. Hennig, G. Lange, D. Krankowsky, D. Offermann, F.J. Schmidlin, U. von Zahn, Vertical density and temperature structure over Northern Euroe, *Adv. Space. Res., 2*, 121, 1983.

Rairden, R.L., L.A. Frank, J.D. Craven, Geocoronal imaging with Dynamics Explorer, *J. Geophys. Res., 91*, 13613-13630, 1986.

Ratkowski, A.J., T.D. Conley, N. Grossbard, The effectsof atmospheric structure on optical sensors, IRIS Target Background Discrimination Meeting, San Diego, February 1986.

Rawer, K., D. Bilitza, S. Ramakrishnan, Goals and status of the International Reference Ionosphere, *Rev. Geophys. Space Phys., 16,* 177-181, 1978.

Rawer, K., J.V. Lincoln, R.O. Conkright (editors), *International Reference Ionosphere— IR179,* Rpt. UAG-82, World Data Center for Solar-terrestial Physics, Boulder, CO, 1981.

Rawer, K., C.M. Minnis, K.B. Minnis, K.B., Serafimov, Towards an improved international reference ionosphere, *Adv. Space Res., 4,* 171 pp., 1984.

Rees, D., T.J. Fuller-Rowell, R.W. Smith, Measurements of high latitude thermospheric winds by rocket and ground-based techniques and their interpretation using a three-dimensional time-dependent dynamical model, *Planet. Space Sci., 28,* 919-932, 1980.

Rees, M.H., *Physics and Chemistry of the Upper Atmosphere, Cambridge University Press,* Cambridge, 1989.

Rees, M.H., and D. Luckey, Auroral electron energy derived from ratio of spectroscopic emissions, 1. Model computations, *J. Geophys. Res., 79,* 5181-5186, 1974.

Robertson, D.C., L.S. Bernstein, P.K. Acharya, R.L. Sundberg, J.W. Duff, S.M. Alder-Golden, M.W. Matthew, M.R. Zakin, P.M. Bakshi, Modeling and analysis of atmospheric radiation in the thermosphere and mesosphere, Spectral Sciences Inc, Burlington, MA, SSI-TR-144, 1988.

Roble, R.G., J.M. Forbes, F.A. Marcos, Thermospheric dynamics during the March 22, 1979, magnetic storm, 1. Model simulations, *J. Geophys. Res., 92,* 6045-6068, 1987.

Ross, M., Delta 181 backgrounds measurements- imager results, presented at Short Wavelength Phenomenology and Applications Conference, Johns Hopkins University Applied Physics Laboratory, 26-28 June, 1990.

Rothman, L.S., R.R. Gamache, A. Goldman, L.R. Brown, R.A. Toth, H.N. Pickett, R.L. Poyneter, J.-M. Flaud, C. Camy-Peyret, A., Barbe, N. Husson, C.P. Rinsland, M.A.H. Smith, The HITRAN database: 1986 Edition, *Appl. Opt., 26,* 4058-4097, 1986.

Rusch, D.W., G.H. Mount, C.A. Barth, R.J. Thomas, M.T. Callan, Solar Mesosphere Explorer ultraviolet spectrometer: Measurement of ozone in the 1.0-0.1 mbar region, *J. Geophys. Res., 89,* 11677-11687, 1984.

Sharmat, R.D., ————————————AFGL-xx-xxxx, 1987.

Sharma, R.D., A.J. Ratkowski, R.L. Sandberg, J.W. Duff, L.S. Bernstein, P.K. Archaya, J.H. Gruninger, D.C. Robertson, R.J. Healey, SHARC, Air Force Geophysics Laboratory, AFGL-TR-89-0229, 1989.

Sharp, W.E., D. Ortland, R. Cageao, Concerning sources of O(1D) in aurora: electron impact and dissociative recombination, *J. Geophys. Res., 88,* 3229-3232, 1983.

Schoberl, M.R., Stratospheric warmings: observations and theory, *Rev. Geophys. Space Phys., 16,* 521-538, 1978.

Schoeberl, M.R., and D.F. Strobel, The zonally averaged circulation of the middle atmosphere, *J. Atmos. Sci., 35,* 577-591, 1978.

Simmons, A.J., and R. Strüfling, Numerical forecasts of stratospheric warming events using a model with a hybrid vertical coordinate, *Quart. J. Roy. Met. Soc., 109,* 81-111, 1982.

Simons, R.E., *Electro-Optics Handbook,* RCA Electronics Components, Tech. Series EOH-11, Electro-Optics Products Operation, Lancaster, PA, 1974.

Solomon, S.C., P.B. Hays, V.J. Abreu, The auroral 6300Å emission: observations and modeling, *J. Geophys. Res., 93,* 9867-9882, 1988.

Stair, A.T., Jr., R.D. Sharma, P.M. Nadile, D.J. Baker, W.F. Grieder, Observations of limb radiance with cryogenic spectral infrared rocket experiment, *J. Geophys. Res., 90,* 9763-9775, 1985.

Starkov, G.V., Analytical representation of the equatorward boundary of the oval auroral zone, *Geomag. Aeron., 9,* 614-xxx, 1969 (in English).

Strickland, D.J., D.L. Book, T.P. Coffey, J.A. Fedder, Transport equation techniques for the deposition of auroral electrons, *J. Geophys. Res., 81,* 2755-xxxx, 1976.

Strickland, D.J., J.R. Jasperse, J.A. Whalen, Dependence of auroral FUV emissions on the incident electron spectrum and neutral atmosphere, *J. Geophys. Res., 88,* 8051-8062, 1983.

Strickland, D.J., R.R. Meier, J.H. Hecht, A.B. Christensen, Deducing composition and incident electron spectra from ground-based auroral optical measurements: theory and model results, *J. Geophys. Res., 94,* 13527-13539, 1989a.

Strickland, D.J., R.P. Barnes, R.J. Cox, D.E. Anderson, Jr., J.F. Carbary, C.-I. Meng, Analysis of UV limb data from low Earth orbit, *Ultraviolet Technology III*, R.E. Huffman, ed., Proc. SPIE 1158, 59-68, 1989b.

Strutt, J.W., On the light from the sky, its polarisation and colour, *Phil. Mag., 41*, 107-120, 1871.

Thomas, G.E., Solar Mesosphere Explorer measurements of polar mesospheric clouds (noctilucent clouds), *J. Atmosph. Terr. Phys., 46*, 819-824, 1984.

Thomas, G.E., and J.J. Olivero, Climatology of polar mesospheric clouds, *J. Geophys. Res., 94*, 14673-14681, 1989.

Turco, R.P., O.B. Toon, R.C. Whitten, R.G. Keesee, D. Hollenbach, Noctilucent clouds: simulation studies of their genesis, properties, and global influences, *Planet. Space Sci., 30*, 1147-1181, 1982.

Ulwick, J.C., K.D. Baker, A.T. Stair, Jr., W. Fringr, R. Hennig, K.U. Grossman, E.R. Hegblom, Rocket-borne measurements of atmospheric infrared fluxes, *J. Atmos. Terr. Phys., 47*, 123-131, 1985.

Vallance Jones, *Aurora*, D. Reidel, Dordrecht, Holland, 1974.

van de Hulst, H.C., *Multiple Light Scattering* (vols. 1, 2), Academic Press, New York, 1980.

Van Zandt, T.E., A universal spectrum of buoyancy waves in the atmosphere, *Geophys. Res., Lett., 9*, 575-587, 1982.

von Zahn, U., and W. Meyer, Mesopause temperatures in polar summer, *J. Geophys. Res., 94*, 14647-14651, 1989.

Watkins, B.J., and R.H. Wand, Observations of clear air turbulaence and winds with the Millstone Hill radar, *J. Geophys. Res., 86*, 9605-9614, 1981.

Walterscheid, R.L., L.R. Lyons, K.E. Taylor, The perturbed neutral circulation in the vicinity of a symmetric stable auroral arc, *J. Geophys. Res., 90*, 12235-12248, 1985.

Walterscheid, R.L., and G.Schubert, Gravity wave fluxes of O3 and OH at the nightside mesopause, *Geophys. Res. Lett., 16*, 719-722, 1989.

Walterscheid, R.L., and L,R, Lyons, The neutral E region zonal winds during intense postmidnight diffuse aurora: response to observed particle fluxes, *J. Geophys. Res.*, *94*, 3703-3712, 1989.

Winick, J.R., R.H. Piccard, R.A. Joseph, R.D. Sharma, P.P. Winterteiner, An infrared spectral radiance code for the auroral thermosphere, AFGL-TR-87, Air Force Geophysics Larboratory, Hanscom Air Force Base, 1987.

Wohlers, M., R. Huguenin, M. Weinberg, R. Huffman, R. Eastes, F. Delgreco, Estimated UV clutter levels at 10-100 meter sensor pixel resolution extrapolated from recent Polar Bear measurements, in *Ultraviolet Technology III*, ed. R.E. Huffman, Proc SPIE 1158, 28-37, 1989.